SYNTHESIS AND CHARACTERIZATION OF NANOSTRUCTURED ZINC OXIDE THIN FILMS USING AQUEOUS CHEMICAL METHOD

BY

APEH, OLIVER OKECHUKWU
PG/MSC/13/66155

DEPARTMENT OF PHYSICS AND ASTRONOMY

FACULTY OF PHYSICAL SCIENCES

UNIVERSITY OF NIGERIA, NSUKKA

SUPERVISORS: PROF. P.U. ASOGWA

DECEMBER, 2015.

TITLE PAGE

SYNTHESIS AND CHARACTERIZATION OF NANOSTRUCTURED ZINC OXIDE THIN FILMS USING AQUEOUS CHEMICAL METHOD

BY

APEH, OLIVER OKECHUKWU
PG/MSC/13/66155

A PROJECT PRESENTED TO THE DEPARTMENT OF PHYSICS AND ASTRONOMY, FACULTY OF PHYSICAL SCIENCES, UNIVERSITY OF NIGERIA, NSUKKA IN FULFILLMENT OF THE REQUIREMENTS FOR THE AWARD OF THE DEGREE OF MASTER OF SCIENCE (MSc) IN SOLAR ENERGY PHYSICS/MATERIALS SCIENCE.

DECEMBER, 2015.

CERTIFICATION

Apeh, Oliver Okechukwu, a postgraduate student in the department of Physics and Astronomy, with registration number PG/Msc/13/66155, has satisfactorily completed the requirement for research work for the degree of Master of Science (MSc) in solar Energy Physics/Materials Science. The work embodied in this thesis is original and has not been submitted in part or full for any other diploma or degree in any other university.

_____

Prof. P. U. Asogwa
(Supervisor)

_____ _____

Prof. J.U. Urama **External Examiner**
(Head of Department)

DEDICATION

This research work is dedicated to Almighty God for His continual guidance and protection throughout the course of these studies. May only His name be glorified now and forever more.

ACKNOWLEDGEMENT

I have great pleasure to express my immense gratitude towards my Supervisor Prof. P. U. Asogwa for his complete guidance coupled with incessant encouragement at all phases of this work. His involvement in the minutes of the details has given this thesis the present form. I am greatly indebted to him.

I am very much thankful to Prof. F. I. Ezema for his encouragement, financial support and providing facilities to carryout the experiment to complete this work. I am also thankful to all my lecturers in the department for their guidance and help during my research work.

It is my great pleasure to thank Dr. S. O. Agbo and Mr. S. O. Ezugwu of Western Ontario University Canada for providing facilities to carryout the characterization with fruitful discussions and constant encouragement in every phase of this work.

I thank all my seniors Mr. Amaechi Ifeanyi, James I. K., Mrs. Chinwe, Mr. Solomon Offiah for their help to me during the experimental work.

I also like to extend my regards to the principal St. Cyprianôs special science school Nsukka, Mrs. Ejimchukwu A.D, the Vice Principal, Mr. Eze U.S and other teachers for the cooperation in the course of my studies.

I owe a special thanks to my mother Mrs. Apeh Juliana O. my brothers and sisters for their prayers and financial support in this program. My thanks also go to my fellow students Aroh Benard, Odo Friday, Balogun Bashiru Bolaji,Kester,Njoku-Achu Nnaemeka and others for our maximum cooperation during our course work and project in this course of studies.

TABLE OF CONTENTS

ABSTRACT

In this work, we report on the synthesis of Zinc Oxide (ZnO), by a cost effective and low temperature aqueous chemical method on conducting glass substrates. The grown nanostructures have been characterized by X-ray diffraction analysis (XRD), scanning electron microscopy (SEM), atomic force microscopy (AFM), optical absorption techniques and Raman spectroscopy. Resistivity of the films was studied with I-V data for the ZnO samples. SEM images show the formation of flower, bud, star, spindle and blades-like morphologies at different deposition time ranging from 15 to 40 minutes. The AFM analysis reveals that the films are dominated by voids with regard to surface topography. The XRD results showed that all films crystallized under hexagonal wurtzite structure and presented a preferential orientation along the c-axis with the maximum crystallite size of 86.33 nm. The average transmittance of all the films increase in the visible region from 32 -75% in a long wavelength domain from 300 ï 1100nm. The extinction coefficient decreases with an increase in wavelength and the band gap energy increases from 3.24 to 3.98eV due to increase in phonon energy. In addition to the vibrational modes from ZnO, the Raman spectra are dominated by the longitudinal optics (LO) between 480 ï 580cm^{-1}. The resistivity of the films decreases as deposition time increases, this shows that ZnO thin films is a good conductor.

CHAPTER ONE

1.0 INTRODUCTION

The first use of the concepts found in nanotechnology was ñThereôs plenty of room at the bottomò, a talk given by physicist Richard Feynman at an American physical society meeting on December 29, 1959. Feynman described a process by which the ability to manipulate individual atoms and molecules might be developed, using one set of precise tools to build and operate another proportionally smaller set, and so on down to the needed scale [1].

The term ñnanotechnologyò was defined by Tokyo science University Professor Norio Taniguchi in a 1974 paper as follows: ñNano technology mainly consists of the processing of, separation, consolidation, and deformation of materials by one atom or by one moleculeò. In 1980 the basic idea of this definition was explored in much more depth by Dr. K. Eric Drexler, who promoted the technological significance of nanoscales phenomena and devices through speeches and the book Engine of creation: The coming Era of Nanotechnology (1986) and Nanosystems: Molecular Machinery, Manufacturing and Computation [2,] and so the term acquired its current sense. Engines of creation: The coming Era of Nanotechnology. Nanotechnology and Nano science got started in the early 1980 with two major developments; the birth of cluster science and the invention of the scanning tunneling microscope (STM). In another development, the synthesis and properties of semiconductor nano crystals was studied; this led to the increasing number of metal and metal oxide nanoparticles and quantum dots [3].

Nanotechnology is one of the frontier areas of science due to its versatile application in various fields. Nanomaterials find applications in the field such as miniaturization in electronics, catalysis, and optics, biological and in the energy sector. In addition, Nanomaterials yield next-generation computer chips, better insulation materials, tougher and

harder nanomaterials cutting tools, elimination of pollutants, high energy density batteries, efficient solar cells, high-power magnets, high-sensitivity sensors, automobiles with greater fuel efficiency.

1.1 Why Nano Materials?

At the nanoscale materials properties are very much different from those at a larger scale. Two principal factors cause the properties to differ significantly from bulk materials: increased relative surface area and quantum effects. These factors can change or enhance properties such as reactivity, strength and electrical characteristics.

1.1.1 Increase in Surface Area to Volume Ratio

First, nanomaterials have a relatively larger surface area when compared to the same volume (or mass) of the materials produces in a larger form. Let us consider a sphere of radius ñrò the surface area and volume of the sphere are given by equations (1.1) and (1.2) respectively. The ratio of these two equations is given in eq (1.3) which indicates the increase in surface to volume ratio with decrease in size.

Its surface area $A = 4\acute{}\ r^2$ 1.1

Its volume $V = (4/3)\ \acute{}\ r^3$ 1.2

Surface area to its volume ratio $A/V = 3/r$ 1.3

Thus, when the radius of the sphere decreases, its surface area to volume ratio increases [4-6].

1.1.2 Quantum Comfinement Effect

Quantum confinement is responsible for the increase in energy difference between energy states and band gap. A phenomenon tightly related with the optical and electronic properties of the materials [7-9]. The quantum confinement effect can be observed once the diameter of the materials is of the same magnitude as the de Broglie wavelength of the electron wave function [10]. When materials are small their electronic and optical properties deviate substantially from those of bulk materials. A particle behaves as if it were free when

the confining dimension is large compared to the wave length of the particle. During this state, the band gap remains at its original energy due to a continuous energy state. However, as the confining dimension decreases and reaches a certain limit, typically in nanoscale, the energy spectrum becomes discrete. As a result, the band gap becomes sized dependent. This ultimately results in a blue shift in optical illumination as the sized of the particle decreases. Specifically, the effect describes the phenomenon resulting from electrons and electron holes being squeezed into a dimension that approaches a critical quantum measurement called excitation Bohr radius. In current application, a quantum dot such as a small sphere confines in three dimensions, a quantum wire confines in two dimensions, and a quantum well confines only in one dimension. These are also known as zero-one and two-dimensional potential wells respectively. In these cases they refer to the number of dimensions in which confined particles can act as a free carrier.

1.2 Nanostructural Zinc Oxide

There are three most important structures representing one-dimenional (ID) nanostructures that are being actively studied in nanotechnology: carbon nanotubes, silicon nanowire and ZnO nanorods/nanowires. ZnO is one of the few dominant nanomaterials for nanotechnology [11]. The absence of a centre of symmetry in its wurtzite structure, along with large electromechanical coupling, results in strong piezoelectric and pyroelectric sensors. Up to now, different nanostructures of ZnO have been reported in the literature.

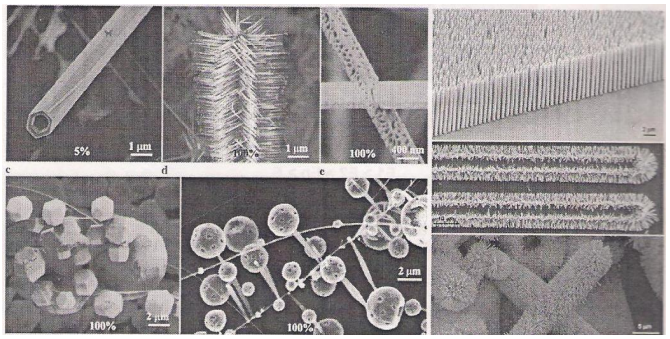

Figure 1.0: Different ZnO nanostructures [11]

Since the discovery of carbon nanotubes, ID materials with various morphologies have stimulated wide interest due to their great potential or fundamental studies of the effects of morphology, dimensionality, and size on their physical and chemical properties [12]. ID nanostructures such as nanowires, nanobelts are ideals systems for investigating the dependence of the electrical and mechanical properties on size and dimensionality. They are expected to play an important role as both interconnect and functional component in the fabrication of nanoscales electronics and optoelectronic devices. Many unique and fascinating properties have already been proposed or demonstrated for this class of materials, such as superior mechanical toughness, high luminescence efficiency, enhancement of thermoelctronic figure of merit, and lowered lasting threshold. [13].

The nanowires have great promise in solar energy conversion compared with conventional planar single crystalline or thin film photovoltaic cells or photo-electrochemical cells, in nonawires, the light absorption and carrier separation occurs in orthogonal direction so solar light absorption occurs along the longer dimensions of the nanowires (microns or more) while the carrier separation occurs by diffusion across the short radial distance (tens of nanometer). As a result, overall device performance does not significantly suffer if lower quality (and less expensive) materials are used [14].

1.3 Growth Mechanisms of ZnO

Spanhel et al [15] have reported that there are two possible ways of describing the growth of ZnO crystals; by Ostwald ripening and by aggregation. Ostwald ripening is an observed phenomenon in solid solutions or liquid sols that describes the change of an inhomogeneous structure over time, that is small crystals or sol particles dissolve and redeposit onto larger crystals or sol particles. In this growth process, as soon as the smallest stable molecular clusters are formed, they rapidly combine to give the next most stable aggregate. The primary aggregates then further rapidly combine to give the next most stable

secondary aggregate and so on.

Meulenkamp[16] suggested that the particle growth in colloidal systems can take place in two ways. The first one corresponds to Ostwald ripening: large particles grow at the expense of smaller particles, which have a higher solubility according to the so-called Ostwaldï Freundlich equation. The second way describes growth by the addition of reactive precursors available in solution to already existing particles. The rate of particle growth is governed by the concentration of precursors or dissolved species and their reactivity, which depends on the number of surface atoms, and the solution composition. Tokumoto et al [17] reported that the formation of ZnO colloidal particles in an alcoholic solvent consists of two stages. During the early stage of phase transformation, small oligomers are continuously formed. At advanced stages, the aggregation of the oligomers leads to crystalline wurtzite, the primary colloidal particles. The primary particles then aggregate and form the secondary colloidal particles. The growth of the colloidal particles is a stepped, discontinuous process which indicates that the predominant mechanism of aggregation is heterogeneous coagulation [18]. This mechanism of growth leads to hierarchical structure.

1.4 Nucleation and Growth

It has been reported by Spanhel [15] that at least four different ñprimary particles or clustersò serving as initiators of the ZnO colloid growth, as precursor, could be identified, such as concentrations, pressure, pH and temperature. The nature of these ñprimary particles or clustersò depends strongly on the synthesis conditions chosen viz. initial salt concentration, the temperature and time of the thermal treatment, the nature of alcohol solvent as well as the humidity, storage and analysis conditions. In other respects, Meulenkamp[16], prepared ZnO nanoparticles by addition of LiOH to an ethanolic zinc acetate solution. He showed that control of the particle size was improved by the influence of temperature, water, and reaction products during the aging of ZnO sols. Water and acetate accelerates the particle growth. Hu

et al [19] has synthesized ZnO nanoparticles by precipitation from zinc acetate in a series of n-alkanols from ethanol to 1-hexanol as a function of temperature.

The kinetics of nucleation and growth are expected to be strongly dependent on the properties of the solvent. For the shorter chain length alcohols, ethanol and 1-propanol, nucleation and growth are retarded compared to longer chain length alcohols, from 1-butanol to 1-hexanol, where nucleation and growth are fast. The particles size increases with increasing temperature for all solvents and increases with alkanol chain length. In fact, during the growth of colloidal ZnO nanoparticles, the alcohols not only provide the medium for the reactions, but also act as ligands to help to control the morphology and particle size of ZnO.

1.5 Crystal Structure of Zinc Oxide

Zinc oxide naturally crystallizes in Wurtzite structure which belongs to the space group $P6_3mc$. The Wurtzite structure is a hexagonal lattice in which each Zn^{2+} ion is tetrahedrally bonded to four O^{2-} ions and viceï versa; this is shown in figure 1.1. In this structure the Zn terminated face (0001) and oxygen terminated face (0001) are the polar faces while the non-polar faces are $(\bar{1}120)$ and $(\bar{1}010$ which contain equal number of zinc and oxygen atoms. The plane perpendicular to the c-axis is called basal planes. Thus there is a polar symmetry along the hexagonal axis. This gives rise to piezoelectricity in ZnO and also plays key role in its crystal growth. The tetrahedral coordination of ZnO indicates the presence of sp^3 hybridized covalent bonding, but the strong ionic character of the Zn-O bond, makes ZnO behave like both covalent and ionic compound. The lattice parameters of hexagonal unit cell are a = 3.2495Å and c = 5.2069Å [20]

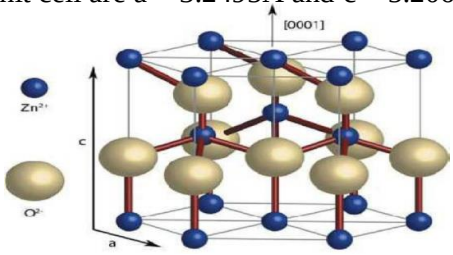

Figure1.1 Hexagonal structure of Zinc Oxide (ZnO) showing the polar faces (perpendicular to c-axis) and non-polar faces (parallel to c-axis) [21].

1.6 Band Structure of Zinc Oxide

The electronic band diagram for wurtzite ZnO is shown in figure 1.2 [22]. The diagram indicates that both the valance band edge maxima and conduction band edge minima occur at k = 0 showing ZnO is a direct band gap semiconductor. It has been found experimentally that due to spinï orbit interaction and crystal-field splitting the valance band in ZnO is split up into three subbands A, B and C, as illustrated in figure 1.2.

The A and C subbands of the valance band are known to posses $\tilde{u}_7$ symmetry and the middle subband B possess $\tilde{u}_9$ symmetry [23]. At 4.2 K the energy band gap of ZnO is 3.43eV

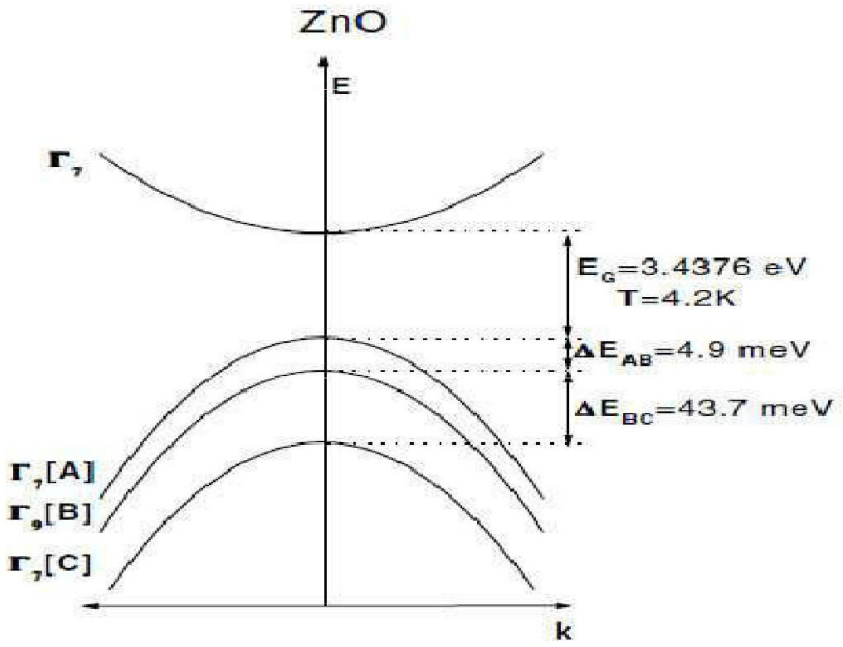

Figure1.2 Band diagram of ZnO showing the splitting of valance band into three subbands A, B, and C due to Crystal field splitting and spin orbit coupling [22].

1.7 Objectives of the Study

The main objectives of this work are;

1. To synthesize the nanostructured ZnO by an aqueous chemical method.
2. To study the effects of deposition time on the thin films.

3. To determine through characterization the morphologies, crystalline structure, optical, and electrical properties of the deposited thin films.
4. To study the effect of copper doping on the nanostructured zinc oxide thin films.

1.8 Research Methodology

Among the methods mentioned in the table 1.1, the aqueous chemical methods are economical and easier than that of the physical methods. But there is no ideal method to prepare thin films, which will satisfy all possible requirements. Among the chemical methods, the aqueous chemical method (ACM) is becoming the most popular and semiconducting thin films can be prepared by this method. It is also popular due to its simplicity, low cost and temperature [18 19]. In this method, the thin films can be deposited on different substrates like glass, ceramics, metalsé .

Table 1.1 *Thin Film Deposition Techniques*

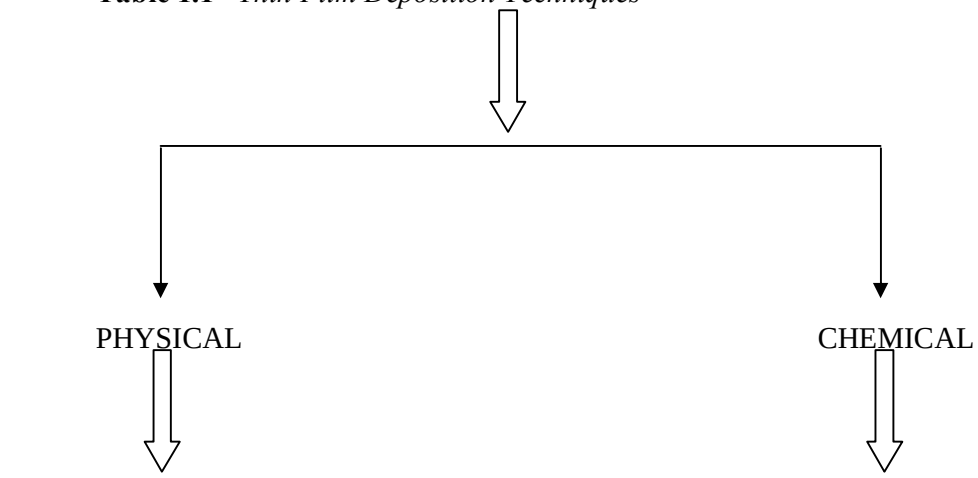

SPUTTERING	EVAPORATION
1. Glow discharge DC sputtering	1. Vacuum Evaporation
2. Triode	2. Resistive heating
3. Getter	3. Flash 4 Evaporation
4. Radio frequency sputtering	5. Electron beam
5. Magnetron sputtering	6. Laser ablation
6. Ion Beam	7. Arc
7. A.C Sputtering	8. R.F. Heating

GAS PHASE	LIQUID PHASE
1. Chemical vaporation Deposition	1. Electro-deposition
2. Laser chemical vapor deposition	2. Chemical bath deposition (CBD)
3. Photo-chemical vapor deposition	3. Electro less deposition
4. Plasma enhanced vapor deposition	4. Anodization 5. Liquid Phase Epitaxy
5.Metal-organo chemical vapor deposition (MO -CVD)	6. Sol-gel
	7. Spin coating
	8. Spray-Pyrolysis (spt) techni polymer assited
	9. Deposition (PAD)
	10. Aqueous Chemical Method

ACM is simple and low cost technique and has capability to produce large area of high quality adherent films of uniforms thickness. In addition to its simplicity, ACM has some advantages;

1. Unlike closed vapor deposition method, ACM does not require high quality targets and /or substrates nor does it require vacuum at any stage which is a great advantage, if the technique is to be scaled up for industrial applications.
2. ACM can produce firms on less robust material because it operates at moderate temperature [100-250^{o}C].
3. By changing the composition of the solution during the deposition process, it can be used to make layered films and the films having composition gradients throughout the thickness.
4. It offers an extremely easy way to dope films with any element in desired proportion by merely adding it in solution form to the deposition solution. However one must be aware of solution miscibility and solubility.
5. The deposition time and hence the thickness of the films can be easily controlled over a wide range (~ 50nm to few microns) by changing the deposition parameters, thus eliminating the major draw backs of chemical method such as sol-gel which produce films of limited thick.

1.10 Aqueous Chemical Method

Nanostructures of ZnO such as nanowires, nanorods, nanocombs, nanorings, nanoloops, nanobows and nanobelts have been reported [24-25]. These nanostructures have been synthesized under controlled growth conditions. ZnO nanostructures can be synthesized either through gas phase synthesis or through solutions phase synthesis. Catalytic growth via the vapor-liquid-solid epitaxial mechanism, CVD, PLD, templating, sputtering and epitaxial electrodeposition have been particularly successful in creating highly oriented arrays of

anisotropic nanorods of ZnO [26]. However these methods have lot of disadvantages such as high cost, tedious operation, it requires vacuum, high temperature, expensive substrate, and rigorous experimental conditions and so on. Among these various methods Aqueous Chemical Deposition method is promising due to simple manipulation, low production cost, does not require vacuum, large scale deposition, unique ability to tune the orientation and morphology and easy upward scale, which have been used to generate a diverse array of ZnO crystals at the micro/nano scale level. By selecting different synthesis conditions such as solvent and Zinc salt, the micro disk and hierarchical ZnO nanostructures can be obtained.

The deposition of metal oxide thin film by aqueous solution method [27] involves controlled precipitation on a substrate via hydrolysis and condensation reaction of metal ions or complexes from aqueous solution. Crystal morphology is strongly influence by experimental conditions such as chemical speciation in the solution, the level of super saturation, the temperature and nature of substrate including pH of growth solution. It is possible to grow ZnO nanorods of different dimensions with the same concentration and the same growth duration simply by varying the pH of the growth solution.

CHAPTER TWO

2.0 LITERATURE REVIEW

Zinc oxide (ZnO) is a group II &VI compound semiconductor having wide band gap of about 3.37 eV. It has large exciton binding energy of 60 MeV at room temperature. It shows piezoelectricity. It is nontoxic material which is cheaply available. Variety of nanostructures of ZnO can be grown. Due to these properties, ZnO is a material of huge technological importance. It has applications in optoelectronic devices such as solar cell [28], optical wave guide [29], light emitting diodes (LED) [30] and transparent thin film transistor [31]. It has been applied in surface acoustic wave (SAW) devices [32].Nanostructures of ZnO have been used as nanogenerators [33] for harvesting energy in nanoscale. All these interesting properties and applications of ZnO have generated a lot of interest its study in thin film as well nanostructured films.

Zinc oxide crystal has native point defect which greatly affects its optical and electrical properties. These defects create electronic states in the band gap which influence its optical emission properties. The grown ZnO crystal has always been found to be n-type. It has been shown theoretically that both oxygen vacancy (V_O) and zinc interstitial (Zn_I) have high formation energies in n-type ZnO and they are deep level donors [34].Thus it is considered that neither V_O nor Zn_I exists in measurable quantity. The search for high conductivity p-type ZnO still remains an active area of research. Hydrothermal solution synthesis [35-36] and electrochemical deposition in porous membranes were investigated to produce oriented ZnO nanorods and tubes respectively. Although oriented nanowires and nanorods have attracted wide attention, the direct fabrication of large arrays of complex nanostructures with controlled crystalline morphology, orientation and surface architectures remains a significant challenge. Various research works have been done on zinc oxide using

different methods.

2.1 Works on Zinc Oxide

Zhengrong et al [37] reported a low-temperature, environmentally benign, solution based approach for the preparation of complex and oriented ZnO nanostructures and the systematic modification of their crystal morphology. By using controlled seeded growth and citrate anions that selectivity adsorb on ZnO, they prepared large arrays of oriented ZnO nanorods with controlled aspect ratios, complex film morphologies made of oriented nanocolumns, nanoplates and complex bilayers showing in situ column-to-rod morphological transitions. Wang et al [38] investigated the photoluminescence of ZnO nanorod arrays on Si substrate. They found strong UV emission and a broad weak green emission. They further investigated the origin of green emission by varying the post treated conditions. Wang et al [39] studied the effect of preparation conditions on the growth rate, morphology and crystallinity of ZnO nanorod arrays on seeded substrates. In particular they found that largest growth rate for $[Zn(NO_3)_2]/[C_6H_{12}N_4]$ ratio =1. They also found the linear increase of radial and axial dimensions of ZnO nanorods with increase in reaction time up to 4 hours. Kenanakis *et al* [40] prepared c-axis oriented ZnO nanorod arrays on seeded glass and si substrates. They found preparation of thin ZnO seed layer is crucial for c-axis orientation. They also found that aqueous solution growth on bare substrates leads to the formation of flower like nanostructures, consisting of randomly oriented nanorods. The grown nanorods were highly transparent in the visible region while the complex nanostructures do not show high transmittance. Shakti *et al* [41] have prepared ZnO nanorods by hydrothermal process and found ultra violet emission at room temperature, the electrical property of nanorods showed rectifying behavior. Gnanasangeetha and SaralaThambavani [42] reported the exploit of aqueous leaf extract of Corriandrum sativum as an eco-friendly agent for the pattern of Zinc Oxide nanoparticle using zinc acetate and sodium hydroxide as a surrogate for Chemical

method. Fourier transform infrared (FT-IR) reveals the presence of phytoconstituents like alcohol, aldehyde and amine which were the surface active molecules that stabilized the nanoparticles.

Kathirvel et al [43] looked at spectral investigations of chemical bath deposited zinc oxide thin films by ammonia gas sensor. The results showed hexagonal structure of X-ray diffraction along with c-axis orientation. They also reported a band edge emission from the film at room temperature. Moradi and Kangarlou[44] produced doped ZnO with Al on glass substrate by chemical bath deposition. The results showed layers of grains of AZO growth with cubic structure and crystalline intensities decreases. Wahab et al [45] studied the effect of pH variation on zinc oxide nanostructures. It was found that the morphology of ZnO nanostructures depends on the pH of the precursor solution. The FTIR spectroscopic measurement of ZnO also comes in the range of 475 to 424 cm^{-1}. Kumar et al [46] synthesized Zinc oxide nanoparticles using a simple precipitation method with zinc sulfate and sodium hydroxide as starting materials. Their SEM images show that the morphology was changed with calcination temperature. They also found that the band gap of ZnO decreased by an increase in calcination temperature, and the absorption maximum is also shifted to higher wavelengths.

Chandramohan et al [47] studied the growth of undoped and metal doped ZnO nanostructures by solution growth, the SEM images reveal continuously stacked nanorods of diameter ranging from 20nm to few hundred nanometers. The AFM studies reveal the surface to be of minimum roughness composed of spherical and hexagonal shaped grains. Ali et al [48] prepared ZnO thin films by chemical bath deposition technique using glass substrates with bath temperature of 80^0C. The X-ray diffraction analysis shows that the prepared samples were polycrystalline and it exhibits hexagonal structure along with c-axis orientation. The crystallite size and band gap were found to change with the annealing temperature (Ta),

the maximum grain size of the film was 60.993 nm at Ta=350^{0}C. Opanasyuk et al [49] investigated the structural and sub-structural characteristics of ZnO films obtained by chemical bath deposition from solutions of zinc sulfate, thiourea and ammonia, the results of the films they generated displayed a hexagonal [002] growth texture, They also found the average size of coherent scatter domain (CSD) in directions corresponding to the axes of the crystal lattice of the hexagonal phase is equal to (L(100) = (21-48) nm, L(002) = (38-60) nm, L(110) = (21-36) nm); it decreases with increasing thiourea concentration in the initial solution.

Byrczek, et al [50] studied the influence of the chemical compounds on the nanostructured zinc oxide growth in chemical bath deposition. The experiments have shown that small addition of the organic compound, namely ascorbic acid (1:5, 5mol into 250 ml of H_2O) change the shape of the structure and decrease its adhesion to the substrate. The samples, where hexamethylenetetramine (HMT, $C_6H_{12}N_4$) was replaced with urea, are different than ZnO structures obtained in the classical way in chemical bath deposition (CBD). Berestok, et al[51] investigated the structural properties of ZnO thin films, they found that growth of thin layers took place by the formation of nanorods as hexagonal prisms and grew perpendicularly to the substrate with further growth of plate crystallites between nanorods. They also showed that the films have a hexagonal structure with lattice constant; varying with increasing thickness. In addition they studied the effect of deposition time on the texture quality of ZnO thin films. Furthermore their results showed that the quality of texture was worsened with increasing deposition time.

2.1 X-Ray Diffraction Technique (XRD)

X-ray diffraction is a very powerful and suitable technique for characterizing microstructure of thin films. It is non-destructive, non contact and provides useful information, such as presence and composition of phase, film thickness grain size and

orientation and strain state. The basic principles of X-ray diffraction can be found in textbooks such as Guinie, Barrett and Massalski [52].

Figure 2.1 shows the schematic diagram of X-ray diffractometer. Diffraction in general occurs only when the wavelength of the wave motion is of the same order of magnitude as the repeat distance between the centres. This condition of diffraction is nothing but Braggôs Law and is given as;

$$2d\sin\theta = n\lambda \qquad 2.1$$

Where d = interplaner spacing, ɗ = diffraction angle, ɔ = wavelength of X-ray, n = order of diffraction.

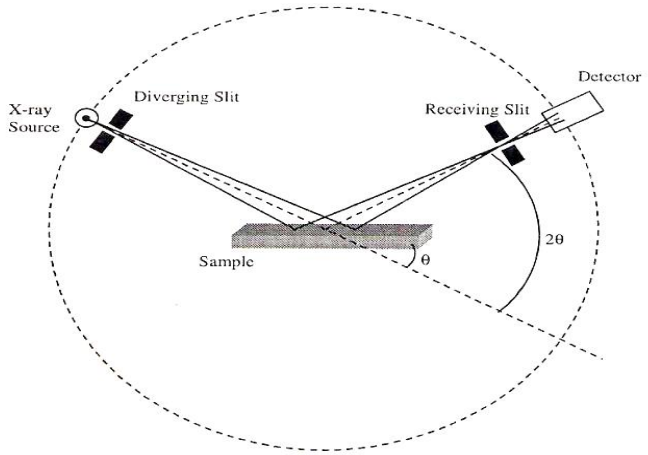

Figure: 2.1 schematic diagram of X-ray diffractometer

In crystalline solids the atoms are ordered in particular repeated pattern referred to unit cell with its intera-atomic spacing comparable to wavelength of X-rays (0.5 to 2.5A). Hence crystals are the best gratings for the diffraction of X-rays. The directions of diffracted X-rays give information about the atomic arrangements and hence the crystal structure and phase formation can be confirmed by X-ray diffraction studies.

The way of satisfying Braggôs condition is devised and this can be done by continuously varying either ɔ or ɗ during the experiment. The way, in which these quantities are varied, distinguish the three main diffraction methods and tabulated in the table.

Table 2.1 X-ray diffraction methods

METHOD	ş	ɗ
Lau method	Variable	Fixed
Rotating crystal method	Fixed	Variable (in part)
Powder method	Fixed	Variable

In powder method the crystal to be examined is reduced to a fine powder and placed in a beam of a monochromatic x-rays. Each particle of the powder is the tiny crystal or assemblage of smaller crystals, oriented at random with respect to the incident beam. Some of the crystals will be correctly oriented so that their (100) planes, for example can reflect the incident beam. Other crystals will be correctly oriented for (110) reflections and so on. The result is that every set of lattices planes will be capable of reflection; this is the principle of powder diffraction.

Ideally, according to Braggôs Law, for the particleôs d values, the constructive interference of x-rays should and occurs only at particular ɗ value i.e Braggôs angle and for all other angles there should be destructive interference and intensity of diffracted beam will be minimum there.

2.3 Identification of Phases

From the d-spacing, phases can be identified in a film using the standard JCPDS powder diffraction file and the reflection can be indexed using miller indices.

However, if the size of the diffracting crystals is small, there is more complete destructive interference at □ ± □□, which broadens the peak corresponding to diffracted beam in proportion to the size of the tiny crystal. This can be used to calculate the particle size. The relation for the same is given by Debye Scherrer and formulated as

$$t = \frac{□.□□}{□ \; □□□□_{□}} \qquad 2.2$$

Where t = particle size, $ɗ_B$ = diffraction angle, ɔ- = wavelength of x-rays and ɓ line broadening at full width at Half Maxima (FWHM).

2.4 Scanning Electron Microscope (SEM)

A scanning electron microscope (SEM) is a type of microscope that produces images of a sample by scanning it with a focused beam of electrons that interact with the atoms in the sample, producing various signals that can be detected and that contain information about the sampleôs surface topography and composition. The electron beam is generally scanned in a raster patter, and the beans position is combined with the detected signal to produce an image [53]. SEM can achieve resolution better than 1 nm. Specimen can be observed in high vacuum, low vacuum, dry conditions (in environmental SEM) and at a wide range of cryogenic or elevated temperatures.

The most common mode of detection is by secondary electrons emitted by atoms excited by the electron beam. On a flat surface, the plume of secondary electrons is mostly contained by the sample, but in a tilted surface, the plume is partially exposed and more electrons are emitted. By scanning the sample and detecting the secondary electrons, an image displaying the topography of the surface is created. Since the detector is not a camera, there is no diffraction limit for resolution as in optical microscopes and telescopes.

A well-focused mono-energetic (~ 25Kev) beam is incident on a solid surface giving various signals. Backscattered electrons and secondary electrons are particularly pertinent for SEM application, their intensity being dependent on the atomic number of the host atoms. Each may be collected, amplified and utilized to control the brightness of the spot on a cathode ray tube. To obtain signals from an area, the electron beam is scanned over the specimen surface by two pairs of electro-magnetic deflection coils and so is the cathode ray rube (C.R.T.) beam in synchronization with this. The signals are transferred from point to point and signal map of the scanned area is displayed on a long persistent phosphorus C.R.T. screen. Change in brightness represents change of a particular property within the scanned

area of the specimen [54]. The ray diagram of scanning electron microscope is shown in figure 2.2

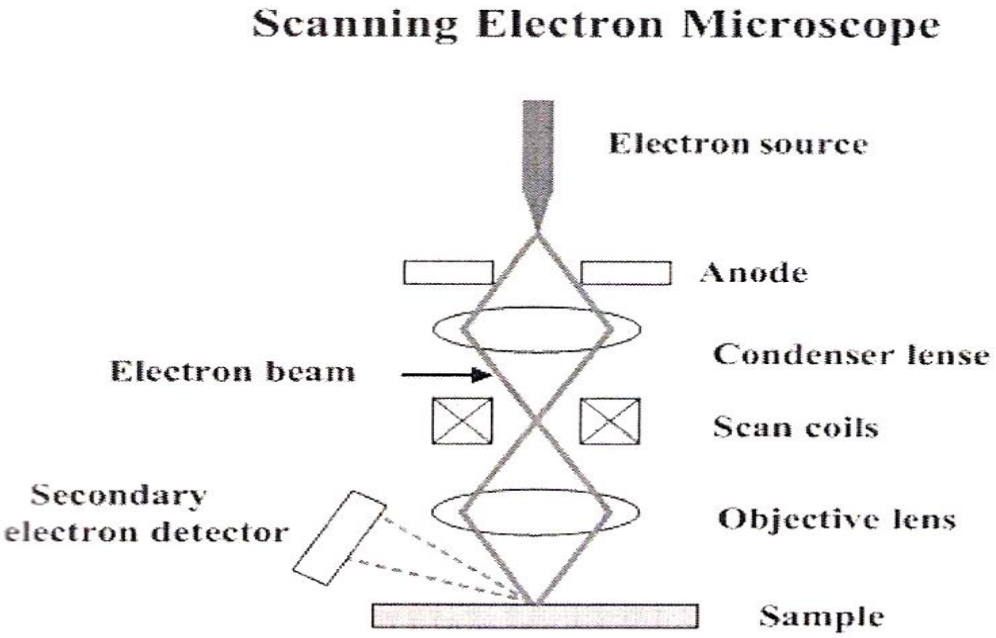

Figure 2.2: Schematic diagram of a scanning electron microscope

Interaction of energetic electron beam with solid surface leads to several signals like elastically scattered electrons (i.e. change of direction without change of energy) from the coulomb field of the nucleus whereas some others includes inelastic scattering of electrons (with change of energy) from the electrons of the host atoms giving rise to secondary electrons.

The scattering cross section for back-scattered electrons is given by [55],

$$\sigma \propto 16.2 \times 10^{-3} \frac{Z^2}{E^2} \qquad 2.3$$

Where, Z = atomic number and E = electric field

2.6 Raman Spectroscopy

Raman spectroscopy named after Sir C. V. Raman is a spectroscopic technique used to observe vibrational, rotational, and other low-frequency modes in a system.[56]. Raman spectroscopy is commonly used in chemistry to provide a fingerprint by which molecules can

be identified. It relies on inelastic scattering, or Raman scattering, of monochromatic light, usually from a laser in the visible, near infrared, or near ultraviolet range. The laser light interacts with molecular vibrations, phonons or other excitations in the system, resulting in the energy of the laser photons being shifted up or down. The shift in energy gives information about the vibrational modes in the system. Infrared spectroscopy yields similar, but complementary information.

Typically, a sample is illuminated with a laser beam. Electromagnetic radiation from the illuminated spot is collected with a lens and sent through a monochromator. Elastic scattered radiation at the wavelength corresponding to the laser line (Rayleigh scattering) is filtered out, while the rest of the collected light is dispersed onto a detector by either a notch filter or a band pass filter.

Spontaneous Raman scattering is typically very weak, and as a result the main difficulty of Raman spectroscopy is separating the weak inelastically scattered light from the intense Rayleigh scattered laser light. Historically, Raman spectrometers used holographic gratings and multiple dispersion stages to achieve a high degree of laser rejection [57]. In the past, photomultipliers were the detectors of choice for dispersive Raman setups, which resulted in long acquisition times. However, modern instrumentation almost universally employs notch or edge filters for laser rejection and spectrographs either axial transmissive (AT), Czernyï Turner (CT) monochromator, or FT (Fourier transform spectroscopy based), and CCD detectors.[58]

There are a number of advanced types of Raman spectroscopy, including surface-enhanced Raman, resonance Raman, tip-enhanced Raman, polarised Raman, stimulated Raman (analogous to stimulated emission), transmission Raman, spatially offset Raman, and hyper Raman.

The Raman Effect occurs when electromagnetic radiation impinges on a molecule and interacts with the polarizable electron density and the bonds of the molecule in the phase (solid, liquid or gaseous) and environment in which the molecule finds itself. For the spontaneous Raman effect, which is a form of inelastic light scattering, a photon (electromagnetic radiation of a specific wavelength) excites (interacts with) the molecule in either the ground rovibronic state (lowest rotational and vibrational energy level of the ground electronic state) or an excited rovibronic state. This results in the molecule being in a so-called virtual energy state for a short period of time before an inelastically scattered photon results. The resulting inelastically scattered photon which is "emitted"/"scattered" can be of either lower (Stokes) or higher (anti-Stokes) energy than the incoming photon. In Raman scattering the resulting rovibronic state of the molecule is a different rotational or vibrational state than the one in which the molecule was originally, before interacting with the incoming photon (electromagnetic radiation). The difference in energy between the original rovibronic state and this resulting rovibronic state leads to a shift in the emitted photon's frequency away from the excitation wavelength, the so-called Rayleigh line. The Raman Effect is due to inelastic scattering and should not be confused with emission (fluorescence or phosphorescence) where a molecule in an excited electronic state emits a photon of energy and returns to the ground electronic state, in many cases to a vibrationally excited state on the ground electronic state potential energy surface.

If the final vibrational state of the molecule is more energetic than the initial state, the inelastically scattered photon will be shifted to a lower frequency for the total energy of the system to remain balanced. This shift in frequency is designated as a Stokes shift. If the final vibrational state is less energetic than the initial state, then the inelastically scattered photon will be shifted to a higher frequency, and this is designated as an anti-Stokes shift. Raman scattering is an example of inelastic scattering because of the energy and momentum transfer

between the photons and the molecules during the interaction. Rayleigh scattering is an example of elastic scattering, the energy of the scattered Rayleigh scattering is of the same frequency (wavelength) as the incoming electromagnetic radiation.

A change in the molecular electric dipole-electric polarizability with respect to the vibrational coordinate corresponding to the rovibronic state is required for a molecule to exhibit a Raman effect. The intensity of the Raman scattering is proportional to the electric dipole-electric dipole polarizability change. The Raman spectra (Raman scattering intensity as a function of the Stokes and anti-Stokes frequency shifts) are dependent on the rovibronic (rotational and vibrational energy levels of the ground electronic state) states of the sample. This dependence on the electric dipole-electric dipole polarizability derivative differs from infrared spectroscopy where the interaction between the molecule and light is determined by the electric dipole moment derivative, the so-called atomic polar tensor (APT); this contrasting feature allows one to analyze transitions that might not be IR active via Raman spectroscopy, as exemplified by the rule of mutual exclusion in centrosymmetric molecules. Bands which have large Raman intensities in many cases have weak infrared intensities and vice versa. For very symmetric molecules, certain vibrations may be both infrared and Raman inactive (within the harmonic approximation). In those instances, one can use a technique of inelastic incoherent neutron scattering to determine the vibrational frequencies. The selection rules for inelastic incoherent neutron scattering (IINS) are different from those of both infrared and Raman scattering. Hence the three types of vibrational spectroscopy are complementary, all giving in theory the same frequency for a given vibrational transion, but the relative intensities giving different information due to the types of interaction between the molecule and the electromagnetic radiation for infrared and Raman spectroscopy and with the neutron beam for IINS.

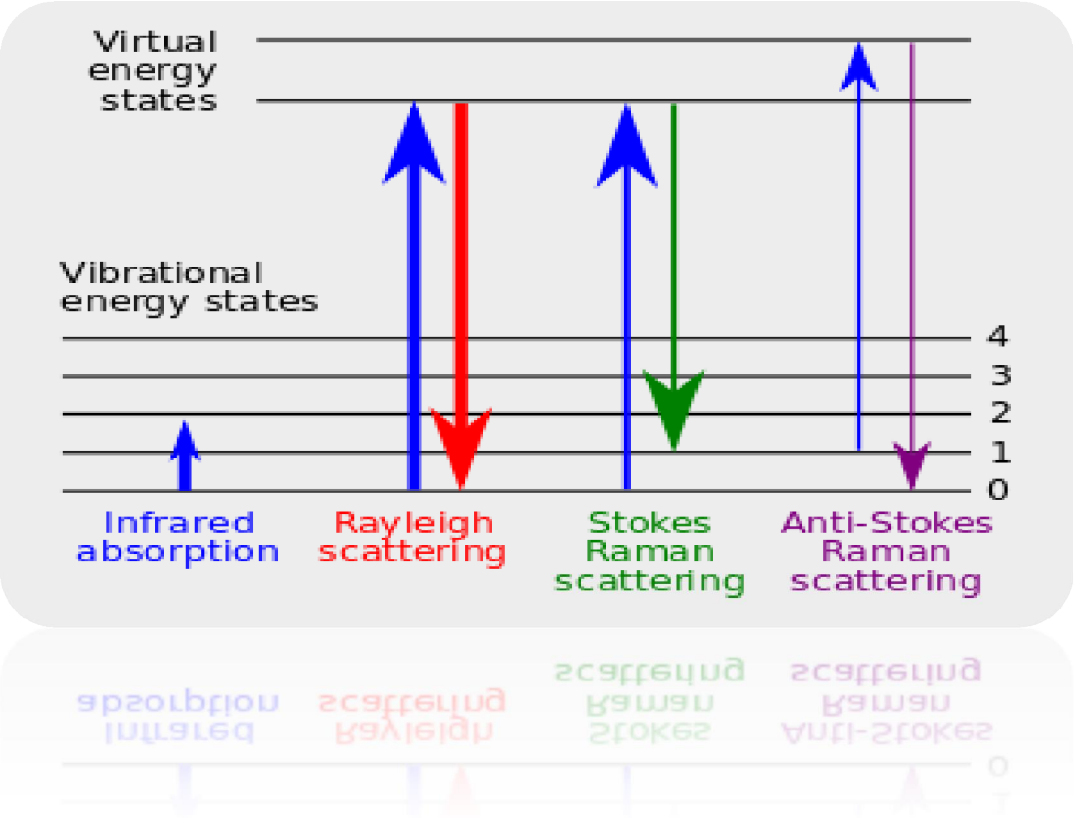

Figure 2.3 Energy-level diagram showing the states involved in Raman signal. The line thickness is roughly proportional to the signal strength from the different transition[59]

Raman spectroscopy is commonly used in chemistry, since vibrational information is specific to the chemical bonds and symmetry of molecules. Therefore, it provides a fingerprint by which the molecule can be identified. For instance, the vibrational frequencies of SiO, Si_2O_2, and Si_3O_3 were identified and assigned on the basis of normal coordinate analyses using infrared and Raman spectra [59]. The fingerprint region of organic molecules is in the (wavenumber) range 500ï 2000 $cm^{ï 1}$. Another way of using the technique is used is to study changes in chemical bonding, as when a substrate is added to an enzyme. Raman gas analyzers have many practical applications. For instance, they are used in medicine for real-time monitoring of anesthetic and respiratory gas mixtures during surgery. In solid state chemistry and the bio-pharmaceutical industry, Raman spectroscopy can be used to not only identify (ID) active pharmaceutical ingredients (APIs), but in the case of multiple

polymorphic forms, it can also be used to identify the polymorphic form of the API. For example there are 4 different polymorphic forms of the API (aztreonam) in Cayston, a drug marketed by Gilead Sciences for cystic fibrosis [60] Both infrared and Raman spectroscopy can be used to identify and characterize the API which is used in the formulation of Cayston. In bio-pharmaceutical formulations, one must use not only the correct molecule, but the correct polymorphic form, as different polymorphic forms have different physical properties, for example, solubility, melting point, and Raman/infrared spectra.

In solid-state physics, spontaneous Raman spectroscopy is used to, among other things, characterize materials, measure temperature, and find the crystallographic orientation of a sample. As with single molecules, a given solid material has characteristic phonon modes that can help an experimenter identify it. In addition, Raman spectroscopy can be used to observe other low frequency excitations of the solid, such as plasmons, magnons, and superconducting gap excitations. The spontaneous Raman signal gives information on the population of a given phonon mode in the ratio between the Stokes (downshifted) intensity and anti-Stokes (upshifted) intensity.

Raman scattering by an anisotropic crystal gives information on the crystal orientation. The polarization of the Raman scattered light with respect to the crystal and the polarization of the laser light can be used to find the orientation of the crystal, if the crystal structure (to be specific, its point group) is known. Raman spectroscopy is the basis for distributed temperature sensing (DTS) along optical fibers, which uses the Raman-shifted backscatter from laser pulses to determine the temperature along optical fibers.

Raman active fibers, such as aramid and carbon, have vibrational modes that show a shift in Raman frequency with applied stress. Polypropylene fibers also exhibit similar shifts. The radial breathing mode is a commonly used technique to evaluate the diameter of carbon

nanotubes. In nanotechnology, a Raman microscope can be used to analyze nanowires to better understand the composition of the structures.

Spatially offset Raman spectroscopy (SORS), which is less sensitive to surface layers than conventional Raman, can be used to discover counterfeit drugs without opening their packaging, and for non-invasive monitoring of biological tissue [61] Raman spectroscopy can be used to investigate the chemical composition of historical documents such as the Book of Kells and contribute to knowledge of the social and economic conditions at the time the documents were produced [62]. This is especially helpful because Raman spectroscopy offers a non-invasive way to determine the best course of preservation or conservation treatment for such materials.

Several research projects demonstrated usage of Raman spectroscopy as a means to detect explosives using laser beams from safe distance [63- 64]. Raman spectroscopy has also been used to confirm the prediction of existence of low-frequency phonons [65] in proteins and DNA [66-67] greatly stimulating the studies of low-frequency collective motion in proteins and DNA and their biological functions [68- 69].

Raman reporter molecules with olefin or alkyne moieties are being developed to allow for tissue imaging with SERS-labeled antibodies [70]. Raman spectroscopy has also been used as a noninvasive technique for real-time, in situ biochemical characterization of healing wounds and multi variants analysis of Raman spectra has enabled a quantitative measure of wound healing progress[66] Raman spectroscopy has a wide usage in studies of biominerals[71]

2.8 Semiconductor Characterization Systems (SCS)

Because of the increasing demand for energy and the limited supply of fossil fuel, the search for alternate sources of power is imperative. Given that there is a vast amount of energy available from the sun; devices that convert light energy into electrical energy are

becoming increasingly important. Solar or photovoltaic (PV) cells convert light energy into useful electrical power. These cells are produced from light-absorbing materials. When the cell is illuminated, optically generated carriers produce an electric current when the cell is connected to a load. A variety of measurements are made to determine the electrical characteristics of PV cells. Characterizing the cells often involves measuring the current and capacitance as a function of an applied DC voltage. The measurements are usually done at different light intensities and temperature conditions. Important device parameters can be extracted from the current-voltage (I-V) and capacitance-voltage (C-V) measurements, such as the conversion efficiency and the maximum power output. Electrical characterization is also important to determine losses in the PV cell. Essentially, characterization is needed to determine ways to make the cells as efficient as possible with minimal losses. To make these important electrical measurements; using a tool such as the model 4200-SCS semiconductor characterization system can simplify testing and analysis. The 4200-SCS is a measurement system that includes instruments for both I-V and C-V measurements as well as software, graphics, and mathematical analysis capability. The software includes tests for making I-V and C-V measurements specifically on solar cells and deriving common PV cell parameters from the test data. This application note describes how to use the model 4200-SCS to make electrical measurements on PV cells.

2.9 Basic photovoltaic cell circuit and device parameters

A photovoltaic cell may be represented by the equivalent circuit model shown in Fig 2.4. This model consists of current due to optical generation (IL), a diode that generates a current [$I_S(eqV/Kt)$], a series resistance (r_s), and shunt resistance (r_{sh}). The series resistance is due to the resistance of the metal contacts, Ohmic losses in the front surface of the cell, impurity concentrations, and junction depth. The series resistance is an important parameter because it reduces both the short-circuit current and the maximum power output of the cell.

Ideally, the series resistance should be 0Ý ($r_s = 0$). The shunt resistance represents the loss due to surface leakage along the edge of the cell or due to crystal defects. Ideally, the shunt resistance should be infinite ($r_{sh} = Ð$).

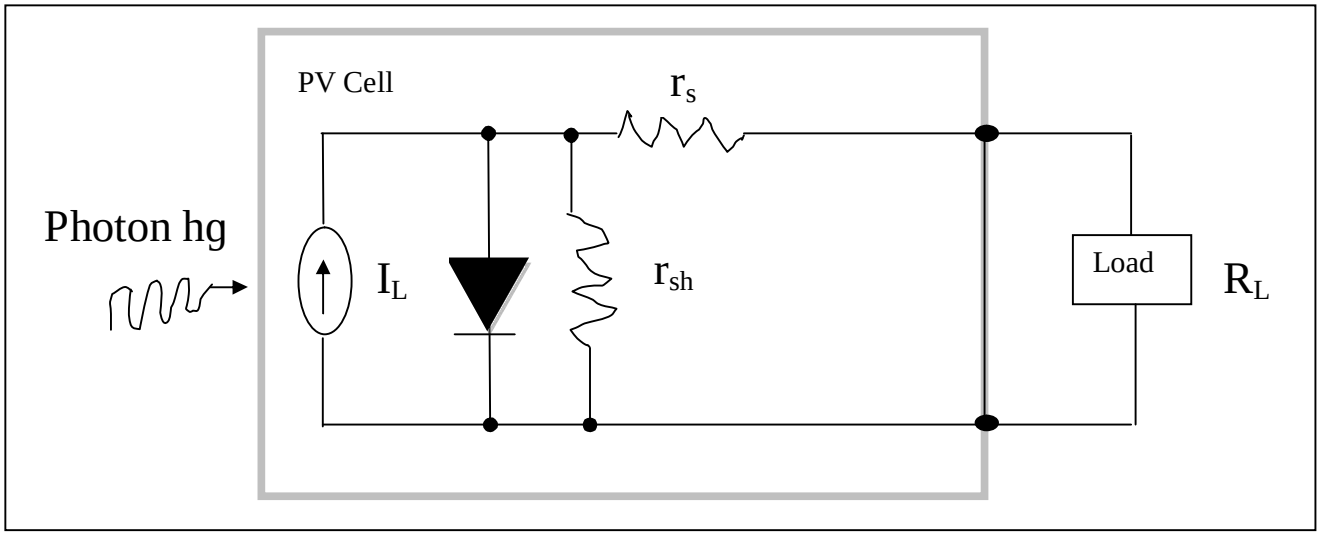

Figure 2.4 Idealized equivalent circuit of a photovoltaic cell

$$I = I_S (e^{qv/Kt} - 1) - I_L \qquad 2.4$$

Where I_s= current due to diode saturation, I_L = current due to optical generation.

Several factors determine the efficiency of the solar cell, including the maximum power point (P_{max}), the energy conversion efficiency (ˇH), and the fill factor (FF). These points are illustrated in figure which shows a typical forward bias I-V curve of an illuminated PV cell. The maximum power point (P_{max}) is the product of the maximum cell current (I_{max}) and voltage (V_{max}) where the power output of the cell is greatest.

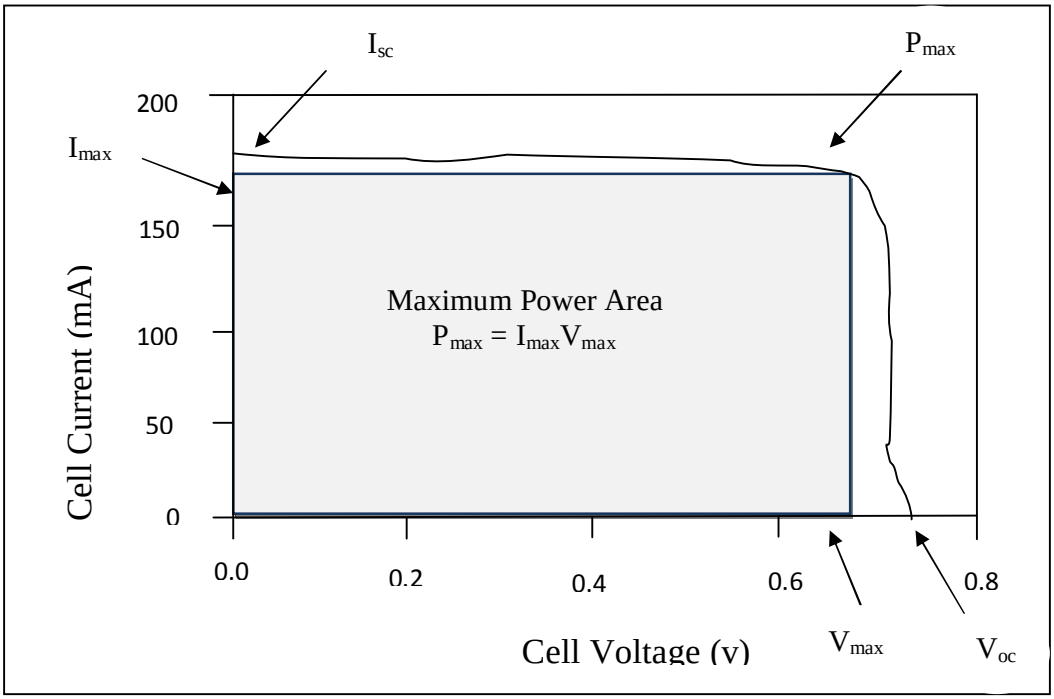

Figure 2.5: Typical forward bias I-V characteristics of a PV cell

2.5 The fill factor is a measure of how far the I-V characteristics of an actual PV cell differ from those of an ideal cell. The fill factor is defined as:

$$FF=\frac{\square\square\square\square\square\square}{\square\square\square\square\square\square} \qquad 2.5$$

Where I_{max} = the current at the maximum power output

V_{max} = the voltage at the maximum power output

I_{sc} = The short- circuit current

V_{os} = the open-circuit voltage

Another important parameter is the conversion efficiency (ˇH), which is defined as the ratio of the maximum power output to the power input to the cell:

$$\eta = \frac{\square\square\square\square}{\square\square\square} \qquad 2.6$$

Where: P_{max} = the maximum power output, P_{in} = the power input to the cell. Is defined as the total radiant energy incident on the surface of the cell.

CHAPTER THREE

EXPERIMENTAL DETAILS

3.0 Experimental set-up:

The schematic of experimental set up employed for the growth of the ZnO films from the aqueous method is shown fig. 3.1. It consists of glass condenser, conical flask, heating mantle and cooling circulation pipes. The substrates were kept in the growth solution.

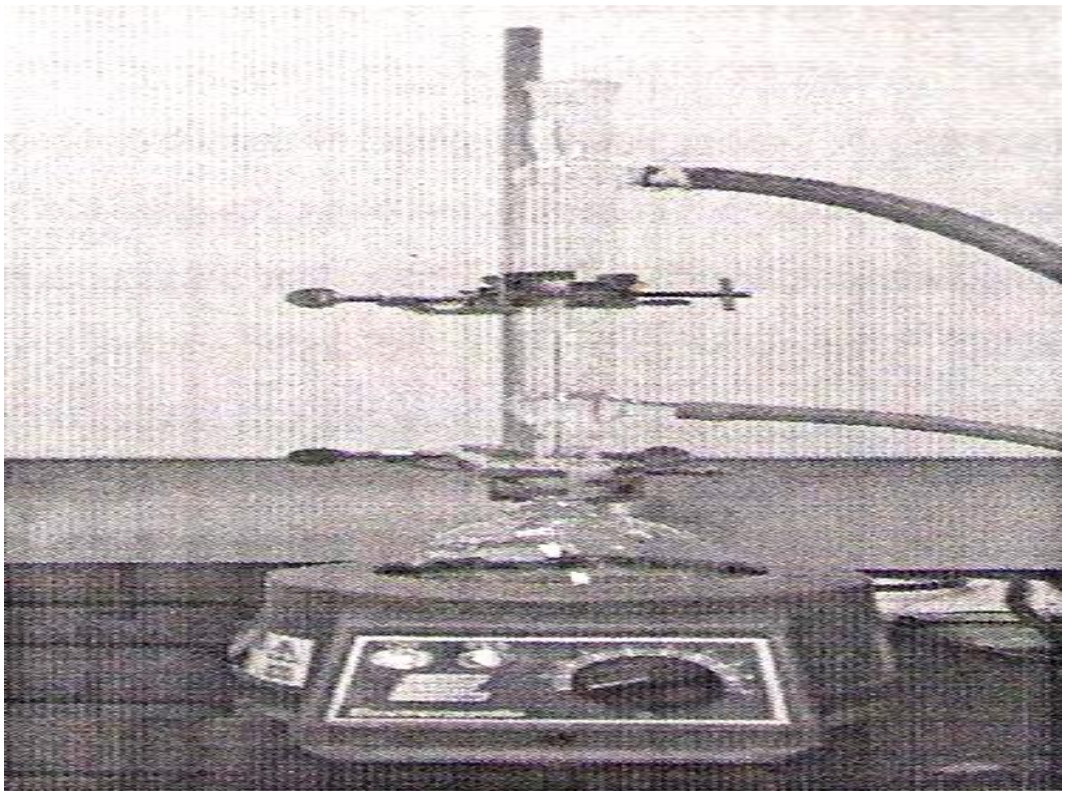

Fig 3.1: Reflux unit

Aqueous chemical method greatly facilitates the growth of one dimensional (ID) ZnO nanostructures by thermal decomposition of hexamethylenetetra-amine (HMTA) and zinc acetate [71]. To initiate the growth from the substrate, a thin layer of ZnO nanoparticles was grown on the substrate by aqueous chemical method. HMTA is a highly water soluble, non-

ionic tetradentate cyclic tertiary amine. Thermal degradation of HMTA releases hydroxyl ions which react with Zn^{2+} ions to form ZnO as follows

$$(CH_3)_6N_4 + 6H_2O \xrightarrow[85^oC]{\triangle} 6HCHO + 4NH_3 + 6H \quad 3.1$$

$$NH_3 + H_2O \longrightarrow NH_4^+ + OH^- \quad 3.2$$

$$Zn^{2+} + 2OH^- \longrightarrow Zn(OH)_2 \quad 3.3$$

$$Zn(OH)_2 \longrightarrow ZnO_{(S)} + H_2O \quad 3.4$$

Reaction Mechanism

$$(i)H_3C-\overset{O}{\overset{\|}{C}}-O-Zn-O-\overset{O}{\overset{\|}{C}}-CH_3 \longrightarrow [CH_3-\overset{O}{\overset{\|}{C}}-O-Zn]^+ + [O-\overset{O}{\overset{\|}{C}}-CH_3] + 2H^+ + 2OH]^- \quad 3.6$$

In above reaction ñzinc-diacetate-dihydrateò is converted into zinc-acetate ion (Cation), acetate ion, photon and hydroxyl anion

$$(ii)\ [CH_3-\overset{O}{\overset{\|}{C}}-O-Zn]^+ + 2OH^- \longrightarrow CH_3COOH + Zn(OH)_2 \quad 3.7$$

In this case the product which is obtained in the above reaction is again converted into acetic acid and zinc hydroxide. The zinc hydroxide leads to ZnO by removing of water molecules, given below.

$$Zn(OH)_2 \longrightarrow ZnO + H_2O \quad 3.8$$

3.1 Preparation of seed solution

In this process, beaker A contains (~ 150ml) of water while beaker B contains (~ 100ml) of the same water. 50ml of ethanol was added in beaker A and 100ml of the same ethanol in B. 1.097g of zinc diethanolamine was added in beaker B and stirred until it dissolves. Also, 0.3ml zinc acetate $Zn(CH_3COO)_2.2H_2O$ was added in beaker A and well

stirred until it dissolves. The solution from beaker B was transferred to A and stirred so as to get uniform and transparent solution. This is called seed solution.

3.2 Seed layer deposition

The slides were first cleaned with cotton wool and put in acetone for about 20 minutes after which the substrates were washed and rinse with distilled water and then dried. The substrates were each dipped into the seed solution for 10s. Then, each was removed gently and dries in air for about 24hrs at room temperature. The coated films were annealed at 350^0C for about 5 minutes to form uniform seed layer on the glass slides.

3.3 Depositions of ZnO thin films

Cleaned beaker and conical flask were both rinsed with distilled water. The seeded substrates were placed vertically in 200ml solution in a conical flask with 0.05M zinc acetate,also 1% of copper was doped into the solution of 0.05M hexamethylenetetramine (HMTA) and stir up until it dissolves, after hexamine was dissolved, we added gradually dissolve zinc acetate solution in it and the conical flask was put inside reflux unit, and then setting the cooling system at 85^0C for 15, 20, 25, 30 and 40 minutes respectively. The refluxed films were washed with distilled water to get rid of loosely adhered material and then air dried at room temperature for characterization.

CHAPTER FOUR

RESULTS AND DISCUSSION

4.1 Scanning Electron Microscopes (SEM)

SEM was carried out to reveal the micro-structural properties of ZnO. This was done using LEO (Zeiss) 1540 field scanning electron microscope (FESEM). The morphologies of the various nanostructures synthesized under different time intervals were examined. It is observed that different shapes of nano films of ZnO were obtained as time intervals changes. Fig 4.1 (a) shows nano- flowers like structures that are spread on the surface. The change in morphology is observed as time varies. Fig 4.1 (b) shows a well-defined nano-flower bud like structures of about 200nm in diameter that are highly uniform and densely packed around the entire surface. Formation of nano-flower bud like morphology is attributed to the strong adsorption of O^{2-} ions on the (0001)-Zn positively charged surface, which reduces the charge density of polar surface. The O^{2-} adsorption stabilizes (0001) surface and promote the growth along the longitudinal direction [72]. Fig 4.1 (c) shows the structures of ZnO doped with Copper. Here, a nano star -like structures of less than 80nm in diameter is observed. We can infer a sharp reduction in nano-sizes which are distributed along the surface. Such reduction in sizes could increase the of mobility electrons there by increasing the electrical conductivity. This is in complete agreement with Pawar et al [73].

Fig 4.1(d) indicates a nano-spindle like structure that is formed on the substrate. The size of the spindle is in the range 250-350nm. Here, ammonia plays a crucial role in the formation of spindle like structure. It provides OH^- ions to form ZnO crystals and also binds metal ions in the solution through equation (3.2) [74]. Finally an increase in nano size is observed in fig 4.1 (e), in this case, a few but irregular clusters of nano-blades (NBs) like structures which are sparsely distributed on the surface is formed. These are composed of size of about 400-600nm. Formation mechanism of nano blade can be explained by precipitation

of $Zn(OH)_2$. At higher time, $Zn(OH)_2$ dissolves and forms Zn^{2+} and OH^- ions in the solution. Hence, the concentration of OH^- ions exceeds the critical value in the solution which forms NBs like structure. [75]

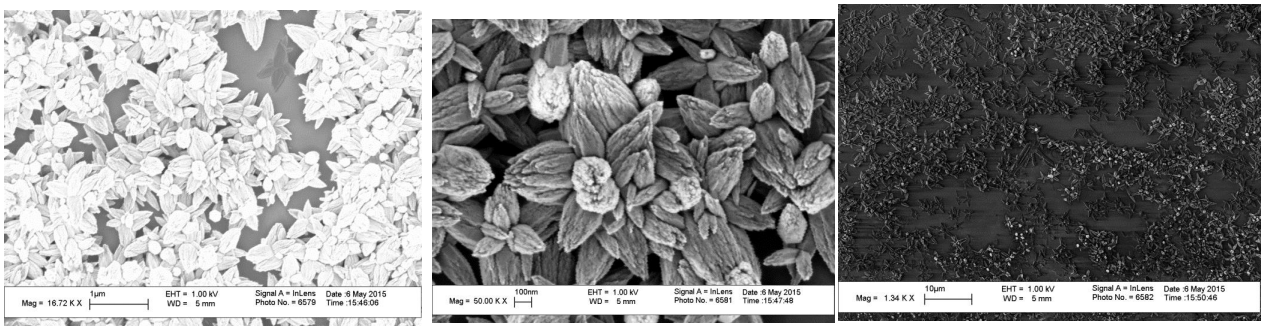

(a) (b) (c)

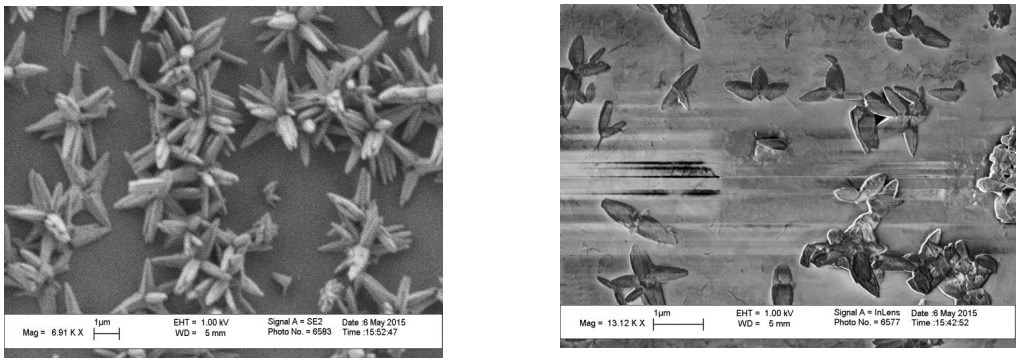

(d) (e)

Figure 4.1: SEM images of the film deposited at different time intervals (a) 15 minutes (b) 20 minutes (c) 30 minutes (d) 25 minutes (e) 40 minutes

Magnifications of 16720

4.2 Atomic Force Microscopy (AFM)

The AFM morphological images, roughness and the thickness were determined on each sample using a Witec Alpha300S atomic force microscope (AFM) operating in tapping mode. These show the surface morphology of ZnO films grown at different time intervals. Fig 4.2(a) shows the films deposited for 15minutes which reveals that the surface is dominated with cone shapes. The change in the surface structures is found when the

deposition time is 20minutes; Fig 4.2(b). In this case, we notice spherical shapes spread around the surface. Fig4.2 (c) shows ZnO films doped with Copper at 30 minutes, here the films are composed of clusters of almost irregular spherical shaped grains with pores. Such porosity favors polycrystalline nanocomposites (PNCs) application as gas sensor since it could aid ion diffusion. This is in agreement with Zhay et al [76]. Figs 4.2 (d) and (e) show the film deposited at 25 and 40 minutes respectively. The images are dominated by voids with regard to surface topography. The transition towards the growth of smooth film was found at 40minutes fig 4.2(e). This change in the growth mode resulted in a substantial reduction of rms roughness 14.0 - 8.0nm fig 4.2(f) [77].

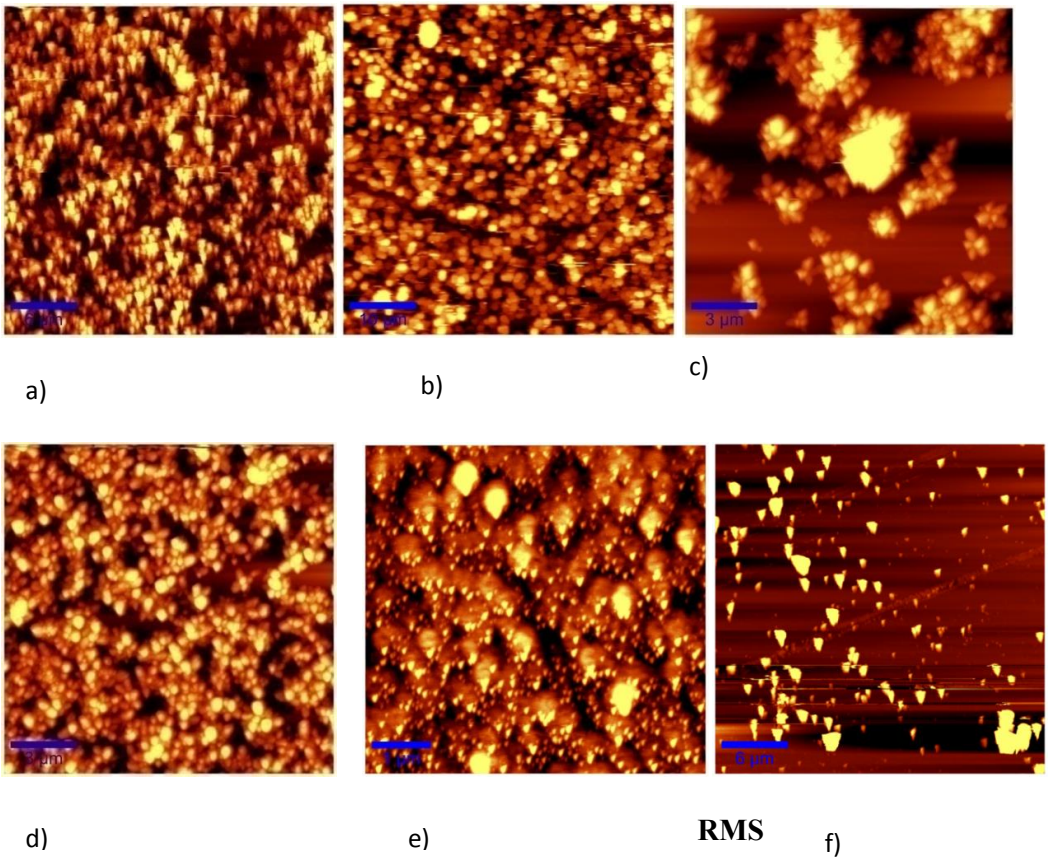

Fig: 4.2 AFM images of the ZnO films

4.3 X-Ray Diffractions (XRD)

The structure and identification of phases were studied with the help of XRD techniques. The figure 4.3 (a-d) show XRD pattern of ZnO annealed at 350^0C for 5 minutes.

It is observed that the ZnO samples were highly oriented, indicating the existence of products with good crystalline structure. All diffraction patterns can be indexed to a hexagonal wurtzite structure, as evidenced by JCPDS data to be (zincite 01-070-2551 phase). In figure 4.3 (a,b&e) ZnO deposited for 25,30 and 40 minutes exhibit major peak along (002) plane close to 34.4371^0,34.1825^0 and 34.4086^0 respectively. Moreover, the much higher relative intensity of the (002) diffraction peak provides evidence that the nanofilms are preferentially oriented in the *c*-axis direction perpendicular to the substrate. The result is in agreement with the report of Pawar et al. [78]

Regarding ZnO nanostructures, the presence of secondary phases and groups were observed. These secondary phases and groups result from the thin substrate film coating on the ZnO films, which served as a seed layer for the nanostructures. Fig 4.3 (c) deposited for 15minutes is influenced by weak intensity radiation. However, figure 4.3 (d) deposited for 20minutes exhibits a strong diffraction along (100) close to 34.4371^0[71].The average crystallite size (D) was calculated from the diffraction line broadening according to Scherrerôs formula [72]

$$\square = 0.9\square/\square\square\square\square \qquad 4.1$$

Where ɓ is the full width at half maximum (FWHM) (in radians). ɔ is the waveleghth of the monochromatic light used (2.29 A) and ɗ is the Braggôs angle in degree. The average crystallite size of the ZnO films is calculated to be 86.33nm. Moreover, presence of broad XRD peaks is an indication of small crystallite size in the nanoscale range affirming the nanocrystalline nature of the films [72].

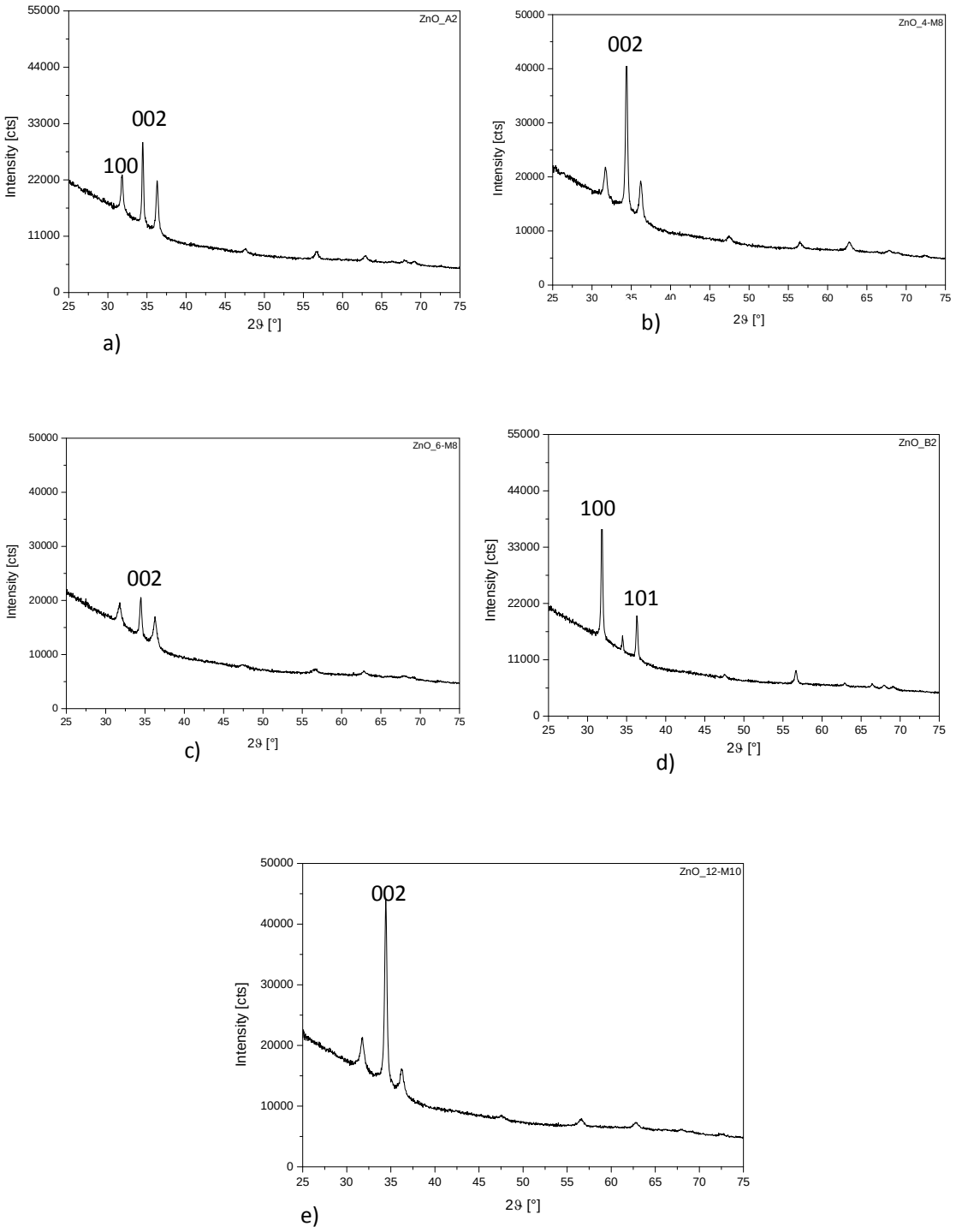

Fig: 4.3 XRD patterns of ZnO deposited at different time

4.4 Optical properties

The UV-vis was investigated using CARY 5E UV-Vis-NIR spectrophotometer. Transmittance of the prepared films were investigated in the wavelength range 300ï 1100nm.

The transmittance of the zinc oxide films are shown in fig 4.4 (c). We noticed a very high transmittance ranging from 32-75% in a long wavelength domain from 300-1100nm. Thus, the transmittance increased within the visible region for transparent ZnO. It is therefore applied in DSSCs because of its usefullness as photoelectrode since the value of transparent is above average in the visible domain. The optical band gap energy (E_g) can be determined by the absorption coefficient (Ŭ) and the incident photon (hv) by the relation

$$\alpha hv = A(E_g - hv)^n \qquad 4.2$$

Where A is a constant, ónô depends on the kind of optical transition that prevails. Specifically, n is ½, 3/2, 2 and 3 when the transition is direct allowed, direct- forbidden, indirect-allowed and indirect-forbidden respectively. In addition, for determining whether a thin film is composed of direct or indirect band gap, a plot of $(Ŭhv)^2$ vs hv is plotted and by extrapolating the linear part of the curve to zero absorption (Ŭ =0) fig 4.4(a). The direct-allowed E_g estimated from the plot is varied ranging from 3.25eV for 15 minutes, for 20 and 25 minutes the E_g is 3.87eV, for 30 minutes, it is estimated as 3.93 eV and the ZnO doped with Cu is 3.98eV with respect to the morphology. The change in E_g is attributed to the crystallite size of the grown structure and morphologies of the sample [80].

The optical extinction spectra were recorded over the range of 300 to 1100 nm. Fig 4.4(b) shows the variation extinction coefficient, K, with wavelength, ø, for all the samples. It is clearly seen that the extinction coefficient decreases with an increase in wavelength and a sharp decrease in extinction coefficient near the band edge indicates better crystallinity of the films.

The thickness of the film was measured by the gravimetric weight differences method using relation;

$\square = \frac{\square}{\square\square\square}$ Where ómô is the deposited films measured by sensitive microbalance; óAô is the area of the deposited film and ógô is the density of the deposited materials in bulk form.

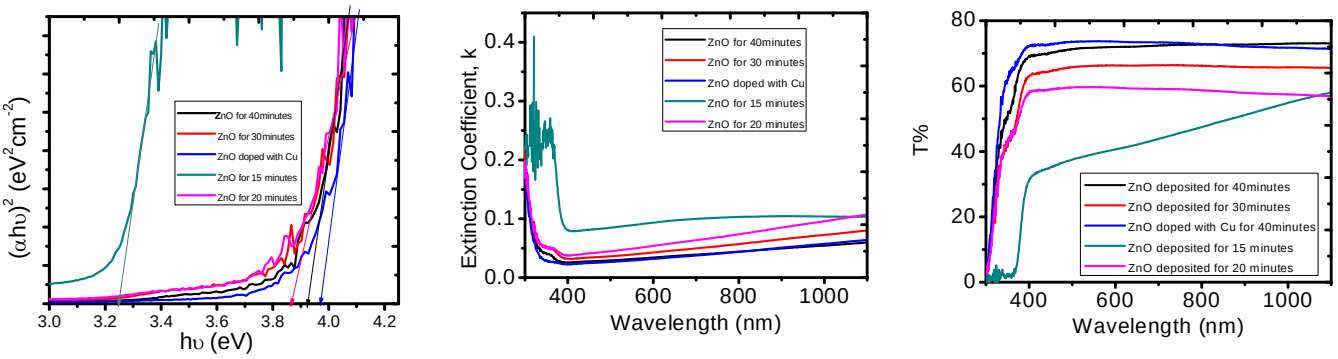

(a) (b) (c)

Fig: 4.4(a) direct energy band gap (b) Extinction coefficient vs wave lenghth (c) Optical transmittance

4.5 Microstructural properties

Raman spectroscopy gives information on vibrational properties of ZnO. It provides qualitative information about the crystallinity of the films. The Raman spectra of this series of ZnO thin films shown in figure 4.5 are dominated by the longitudinal optical(LO) vibrations around 443cm^{-1} and 561cm^{-1} for the figure 4.5 (a) deposited for 15 minutes and the figure in (c) deposited for 20 minutes LO are 340 cm^{-1},443 cm^{-1} and 569 cm^{-1} while that of (b) deposited for 40 minutes is found to be 480cm^{-1},558 cm^{-1},and 793 cm^{-1} respectively. This range is in a complete agreement with Cerqueira [81].The minor peaks at about 590cm^{-1} for figures 4.5 (a) and (c) and 790cm^{-1} for figure (b) seen in the spectrum of pure ZnO has been attributed to the second-order Raman processes involving acoustic phonons. Its presence demonstrates a good quality of the samples [82]

The peaks in the range 480cm $^{-1}$ and 580cm^{-1} reproduce quite well the glass substrates contribution. The narrow peaks centered 590cm^{-1} and 790cm^{-1} is attributed to ZnO crystallites while the broad peaks is characteristics of disordered phase[83] The improvement of crystallinity observed in Raman spectra with increasing time is also observed by X-Ray diffraction, from the increase of the intensity of the (002) peak. It is correlated with an

increase of the crystallite size deduced from X-Ray diffraction analyses (Fig.4.3) above, which is attributed to an increase in surface diffusion of the adsorbed species [83-89].

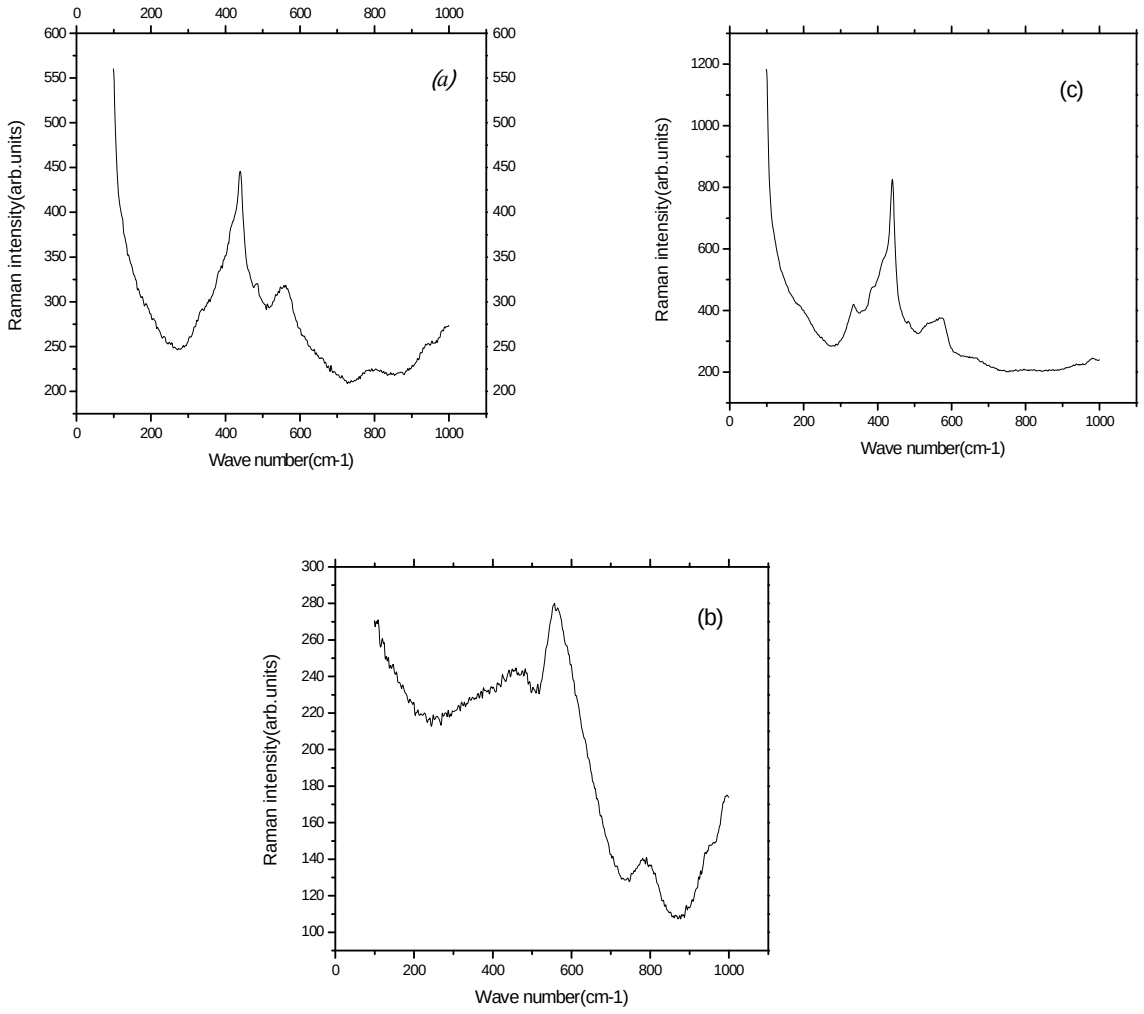

Fig4.5 Raman spectra of ZnO thin films deposited for (a)15 minutes (b) 40 minutes and (c) 20 minutes

4.6 Resistivity studies

The obtained I-V data for the ZnO samples were used to obtain the resistivity of the thin films. The current-voltage curves of the thin films are shown in figure (4.6) below. In order to estimate the resistivity of a sample, we determine the resistance, R using the slope ,S from the I-V plots from the relationship,

$$R = \frac{V}{I} \qquad 4.3$$

Using the average resistance for a sample, we determine the resistivity, ρ with the following formula

$$\rho = \frac{R.A}{L} = \frac{R.Wt}{L} = R.t \qquad 4.4$$

Where R is the resistance of the thin films with thickness t and length L.

The average thicknesses of the films are estimated from the AFM topography maps shown above. This is obtained by placing a cursor to different places on each of the AFM images and thus we found the average of the thickness of each sample. The same procedure was adopted to estimate the resistivities of the other samples.

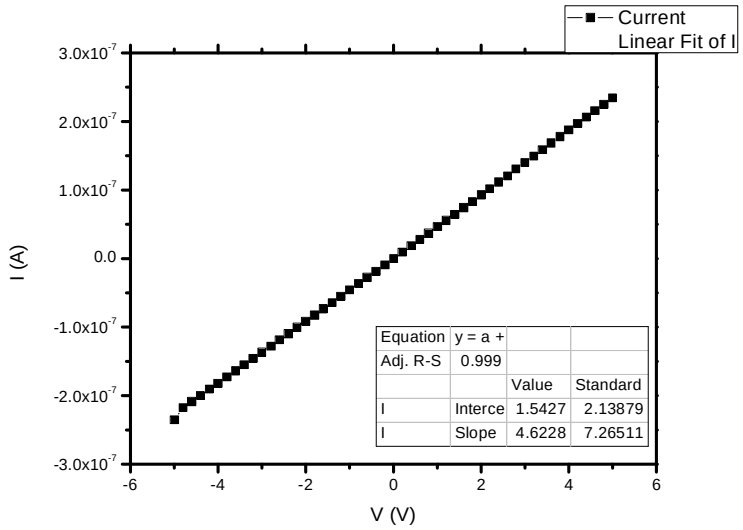

Fig 4.6 A graph of current (I) against voltage (V) for ZnO deposited after 20minutes

Figure 4.7 below shows a graph of resistivity (⍰) against time (T). It is observed from the graph that as the time of deposition increases the resistivity is decreasing. The longer the time the lower the resistivity. Since resistivity is the reciprocal of conductivity, it therefore shows that as the deposition time increases the conductance of ZnO becomes high and attributes to increase in the nano sizes of ZnO as observed in the SEM images in figure 4.1. The graph shows a very high conductance when the time is 30 minutes.

Table 4.1 summarizes the measured values of resistance (R), thickness (t) and resistivity (⍰) for ZnO nanostructure with different deposition time (T)

Table 4.1

Samples	**Deposition time (T)(s)**	**R (Ω) x 10^6**	**t (nm)**	**⍰ (Ωm) x 10^9**
O_2	15.0	9.0	681.22	6.14
O_3	20.0	7.3	247.27	1.81
O_4	25.0	6.7	118.55	0.80
O_5	30.0	9.9	160.23	0.60

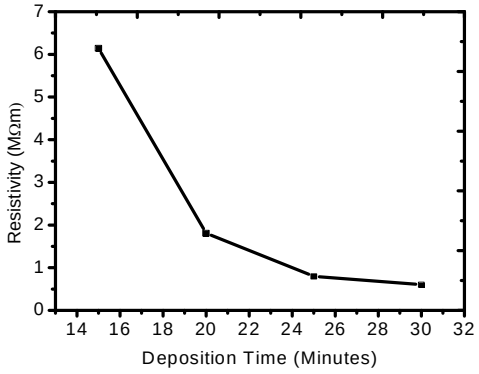

In our investigations we found that almost many of the work reported have the same view with us. Closely, Berestok et al [51] studied the effect of deposition time on texture quality of ZnO using (CBD) but we studied the effect of deposition time on ZnO using aqueous chemical method. Also, we reported the micro structural (Raman spectroscopy) studies on ZnO on both glass substrates and on thin films but some of the reports in the literature we got were on ZnO thin film alone, they did not compare them with glass substrates. Uniquely, in our research, we went further to compare the resistivity studies of ZnO thin films with deposition time. This study has not been found in literature.

CHAPTER FIVE

CONCLUSION

In this research, ZnO was successfully synthesized by aqueous chemical method at relatively low temperature. The structural, morphological and optical properties were investigated using X-ray diffraction (XRD), scanning electron microscopy (SEM) and UV-visible infrared spectroscopy respectively. The morphology of the films shows a dominant nano-flower like structures that increases in size with an increase in deposition time. This is suitable for fast electron transportation and a crucial requirement for photoelectrochemical. The XRD pattern shows highly oriented peaks at (002) and other minor peaks. These confirm high crystalline quality of ZnO with hexagonal wurtzite structure. The bang gap energies determined, ranges from 3.24-3.98eV. Its high transparency is applied in dye sensitized solar cells and photoelectrodes. The Raman spectroscopy revealed a strong dependence of the spectral features upon the nature and concentration of impurities present in ZnO samples. Some of these features can be associated with local impurity vibrational modes while some may be due to structural changes or impurity-induced lattice defects, grain size or secondary phases present in ZnO materials. The graph of resistivity against time decreases with an increase in time thus showing a good conductance.

REFERENCES

[1] D. Mary Archer *Photo electrochemical,* 7 (2010) 3-8
[2] B. David Mitzi, A John, *Inorganic materials,* 9 (2010) 33-57
[3] P.K. Palanisamy, *Applied physics*, 55 (2001) 2
[4] H.Singh Nalwa, *Academic press* 101(2009) 15
[5] T. pradeep, *Tata mcgraw-hill publishing company* (2010)
[6] A.P.Shpak, S.I. Pokutnyi, Y.A.kyi, *Institute of metal physics* (2004)
[7] D.Bimberge, F.Tekhn. *Poluprovod.* 33 (1999) 1044.
[8] M.H. Huang, Y.Wu, H.Feick, N.Tran, E.Weber, P. Yang, *Adv. Mater*. 13 (2001)113.
[9]Z.W. Pan, Z.R. Dia, Z.L. *Wang, Science* 291 (2001) 1947.
[10] J.Y. Li, X.L. Chen, H.li, M. He, Z.Y. Qiao, J. *Crystal. Growth* 233 (2001) 5.
[11]M. Alexe, S. Senz, M. A. Schubert, D. Hesse, U. Gosele, *Advanced Mater.* 20 (2008) 4021.
[12]P.Yang, H.Yan, S.Mao, R.Russo,J.Johnson,R.Saykall,*Advanced.matter*.12 (2002) 323
[13]C.Geng, Y.Jiang, Y.Yao,X.Meng, J.A.Zapien,C.S.Lee, Y.Lifshitz, S.T,Lee,*Advanced. Functional.Matter* 14(2004) 589.
[14]D.Andeen,J.H.Kim,F.F.Lange,G.K.L. Goh,
S.Tripathy,*Advanced.Functional.Matter*.16(2006) 799.
[15]L. Spanhel, J. *Sol–Gel Science Technol*. 39 (2006) 7.
[16] E.A. Meulenkamp, J. *Physics. Chem.* B 102 (1998) 5566.
[17] M.S. Tokumoto, S.H. Pulcinelli, C.V. Santilli, A.F. Craievich, J. *Non-Cryst. Solids* 247 (1999) 176.
[18]C. Jagadish, & S.J. Pearton, *Apply.phyics*,3 (2007) 2.
[19] Z. Hu, G. Oskam, P.C. Searson, J. *Colloid Interface Science.* 263 (2003) 454.
[20]L.K. Van Vugt thesis *Optical properties of semiconducting nanowires 5(2007)105*
[21] J.Y.Park, D.J. Lee, Y.S.Yun, J.H.Moon, B.T.Lee, S.S.Kim, J. *Crystal.Growth,* 276, (2005)158.
[22]E. Fortunato, A. Goncalves, A. Marques, A. Viana, H. Aguas, L. Pereira, I. Ferreira, P.Vilarinho, R. Martins, *Surf. Coat. Technol.*, 180 (2004) 20.
[23]A.Fujishima,K.Honda,*Nature* 238(1972) 737
[24] B.OôRegan,M.Gratzel, *Nature* 353 (1991) 737
[25]M.Gratzel,*Mrs bull* 30 (2005) 23
[26] D.B.Kuang, C.Klein, J.E.Moser,R.Humphry-Baker, N.Evans, Duriaux,S.M.Zakeeruddin,M.Gratzel,*Advanced. Mater*.19(2007) 1133
[27] D.B.Kuang, P.Wang,S.Zakeeruddin,M.Gratzeel ,*Journal.Chem.Soc*.128 (2006) 7732
[28]M.Gratzel,*Chemistry.Letert.* 34(2005) 8
[29]P.Yu, Z.K. Tang, G.K.L.Wong, M. Kawasaki, A. Ohtomo, H. Koinuma, Y. Segawa, *J.Crysalt. Growth,* 184-185 (1998) 601.
[30]A. Tsukazaki, M. Kubota, A. Ohtomo, T. Onuma, K. Ohtani, H. Ohno, S.F. Chichibu, M. Kawasaki, Jpn. J. *Applied. Physics*., 44 (2005) L643.
[31]B. J. Norris, J. Anderson, J. F. Wager, D. A. Keszler, *Journal.Physic*s.36 (2003) 105.
[32]F.S. Hickernell, J. *Appliedl. Physics*,44 (1973) 1061.
[33]Z. L. Wang, *Journal. Song, Science,* 312(5771) (2006) 242.
[34]A.F.Kohan, G. Ceder, D. Morgan, C.G. Van de Walle, *Physics. Review*.B, 61(2000) 15019.
[35]C.G. Van de Walle, *Physics. Review. Letter.*, 85(2000) 1012.
[36]X.S.Wang, Z.C.Wu, J.F. Webb, Z.G. Liu, *Applied. Physics.* A, 77(2003) 561.

[37]R.Zhengrong., Tian, A.James, Voigt, J. Liu, B. Mckenzie, J.Matthew , Mcdermott, A. Mark, Rodriguez, H. Konishi and H. Xu, *Natural. Mater.*, 2 (2003) 821.
[38]M. Wang, C.Hui Ye, Ye Zhang, G. Hua, H. Wang, M. Kong, L. Zhang, *Journal.Crystal. Growth* 91(2006) 334.
[39] S. Wang, T. Tseng, Y. Wang, C. Wang, H. Lu,W. Shih, Int. *Journal.Applied. Ceram. Technol.*, 5 (5)
(2008) 419.
[40] G. Kenanakis, D.Vernardou, E. Koudoumas, N. Katsarakis, *Journal.Crystal.Growth,* 311(23)(2009) 4799.
[41] N. Shakti, Sunita Kumari, P.S. Gupta, *Journal.Ovon. Res.* 7(3) (2011) 51.
[42]D.Gnanasangeetha and D.SaralaThambavani. *Research journal of Material Sciences* Vol.1(7) (2013),1-8.
[43]P. Kathirvel, D.Manoharan , S.Mohan, S. Kumar *Journal of optoelectronics and biomedical Material* Vol.1(1) (2009) 25-33.
[44]S. Moradi and H. Kanarlou *Journal of Fundamental and Applied Life Sciences Vol.5 (1) (2015), 2819-2821.*
[45]R.Wahab, Y.Kim H.Shin *Materials Transactions,* Vol. 50,(8) (2009) 209 ï 2097.
[46]S. Kumar, P. Venkateswarlu, V. Rao G. Rao *International Nano Letters*Vol.3 (30) (2013),2
[47]R. Chandramohan, T.Vijayan J.Thirumalai *International Nano Lettersz* Vol.2(3) (2010) 326
[48]M. Ali. *Journal of Basrah Researches Sciences* Vol. 37. (3) (2011).
[49] A. Opanasyuk, T. Berestok, P.Fochuk, A.Bolotnikov, R. James *International Nano Letters(4)2009)23-27.*
[50]M.Byrczek, M.Malewicz, G Halek and H.Teterycz *acta physica polonica* Vol.116 (2009)
[51]T.O. Berestok, D.I. Kurbatov, N.M. Opanasyuk, A.D. Pogrebnjak,,O.P. Manzhos, S.M. Danilchenko *journal of nano- and electronic physics* vol. **5 (**1) (2013)4.
[52]R.A. Marcus,Annu. Rev.Phy.Chem. 15 (1964) 155
[53]O.D.McMullan and K.C.A.Smith.Advanced Phy.Suppl. 16.(1985) 443.
[54]C.R. Brundle and A.D. Baker *Pergamon press* 2(1978) 1
[55]T.H. Gfoerer, *Method of contact angles* (2000) 9209
[56]A.Smekal, *Die Naturwissenschaften 43(1923)* 873ï 875.
[57]Placzek G.: "Rayleigh Streuung und Raman Effekt", In: Hdb. der Radiologie, Vol. VI., 2, 1934, p. 209
[58]R.K Khanna, *Journal of Chemical Physics* **74** (4): 2108.
[59]S. Marcet *Photonics North* 10 (2012)1117
[60]W.Robin,M. Havener (December 2011) *ACS Nano* **6** (1)(2011) 373ï 77
[61]
[62]K. Anupam,K Shiv E. TayroN. John *Applied Spectroscopy* **66** (11) (2012)444
[63]A.Chou, K.Chen, E. Chen, N.Yi. *Scientia Sinica* **20(1977)** 447ï 457.
[64]H.Urabe, D. Tominaga, K. Kubota, (1983) *Journal of Chemical Physics* **78**(1983) 5937ï 5939.
[65]K.C Chou, *Biochemical Journal* **215**(1983) 465ï 469.
[66] K.C.Chou, *Biochemical Journal* **221**(1984) 27ï 31.
[67]H.Urabe,Y. Sugawara, M. Ataka, A. Rupprecht, *Biophys J* **74**(1998)1533ï 1540.
[68] C.Chou, K.Chen *Biophysical Chemistry* **30**(1988) 3ï 48.
[70]K.C.Chou, *Trends in Biochemical Sciences 23(1989)322*
[71]S.Schlücker, *Journal of Biophotonics* **4** (6) (2011) 453ï 463.
[72]R. Jain, *Analytical Chemistry* **86** (8)(2014) 3764ï 3772.

[73] R.C. Pawar, J.S. Shaikh, P.S. Shinde, P.S. Patil, *Materials Letters* 65 (2011) 2225 ï 2237.
[74]R.Zaera, J. Wang, G.Clement, *phy. Chem.*111,(2007) 16706-1700.
[75] S.U. Offiah, S.C. Ezugwu, F.I. Ezema, O.U. Oparku, P.U. Asogwa, *Journal of Ovonic Research* Vol 6, no 3(2010) P. 135 ï 141.
[76] J.P.Zhay, L.D. Zhay, L.Q. Zhu, Y.Zhay, M.Liu and X.J. Wang,*Applied Physics* 102,
[77] P. Li, H. Liu, Y..Zhang, Y.Wei, X. Wang, *Mater,Chem. Phy.* 106,(2007) 63-69. (2007)114903.
[78]R.C. Pawar, J.S. Shaikh, A.A.Babar.P.M.Dhere, P.S. Patil, *Solar Energy* 85 (2011) 1119-1127.
[79] S.C. Ezugwu, F.I. Ezema, R.U. Osuji, P.U. Asogwa, A.B.C. Ekwealor and B.A. Ezekoye, *Optoelectric and Advanced materials-Rapid Communications,* 3 (2) (2009) 141.
[80] N.Samaele, P.Amornpitoksuk, S. Suwanboon, *powder Technol,* 203 (2010) 243-247.
[81]M.F. Cerqueira, M.I. Vasilevskiy, F.Oliveira, A.G. Rolo, T.Visereu, J.Ayre de decampos, E.Alves, R.Correia, *App.phy.A,*3(2012) 2768.
[82] Z.L.Wang, J.H.Song, *Science* 312, (2006) 242.
[83] L.Vayssieres, K.A Keis, S.E Lingdquist, A. Hagfeldt, *J.Phys. Chem.* B 105 (2001) 3350.
[84] J.J.Wu, S.C.Liu, *J. Phys. Chem.* B 106, (2002) 9546.
[85] Y.S. Zhang, L.S. wang, X.H. Liu,Y.J.Yan, C.Q. Chen, J. Zhu, *J.Phys. Chem.*B 109, (2005) 13091.
[86] J.S. Jie, G.Z. Wang, Q.T. Wang, Y.M. Chen, X.H. Han, X.P. wang, J.G. Hou, *J. Phys. Chem.* B 108, (2004) 11976.
[87] M.J. Zheng, L.D. Zhang, G.H. Li, W.Z. Shen, *Chem. Phys. Lett.* 363, (2002) 123.
[88]C.I.Amaechi.,P.U.Asogwa.,A.B.C.Ekwealor.,R.U.Osuji.,M.Maaza.,F.I.Ezema.,App.phys. A., 117 (2014) 1589.
[89]C.Charpentier, .P.Prod homme, I.Marin, M.Chaigneau, P.Rocacabarocas, *photovoltaic* 2 (2011) 250

REFERNCES

[1] Nanostructures and photo electrochemical systems or solar conversion Editors, Mary D. Archer, Imperial College, UK, Arthur J Nozik National Renewable Energy Laboratory, USA Imperial College Press

[2] Solution processing of inorganic materials, Edited by David B. Mitzi, A John Wiley and Sons Inc. Publication

[3] Nanostructures and Nanomaterials: Synthesis, Properties and Applications, Guozhong Cao, university of Washington, USA USA Imperial College Press

[4] Applied Physics, P.K. Palanisamy, Scitech publications pvt.ltd.

[5] Handbook on Nanostructured materials and Nanotechnology, Edited by Hari Singh Nalwa, Academic press USA.

[6] Nano: the essential, Understanding Nanoscience and Nanotechnology T. pradeep, Tata McGraw-Hill Publishing Company limited New Delhi.

[7] A.P.Shpak, S.I. Pokutnyi, Y.A. kyi,Diagnostics of nanaosystems Semiconductor, Quasi-zerodimensional systems [in Ukrainian], G.V. kurdyumov institute of metal physics of NAS of Ukraine, kyiv (2004)

[8] D.Bimberge, F.Tekhn. Poluprovod. 33 (1999) 1044.

[9] M.H. Huang, Y.Wu, H.Feick, N.Tran, E.Weber, P. Yang, Adv. Mater. 13 (2001) 113.

[10] Z.W. Pan, Z.R. Dia, Z.L. Wang, Science 291 (2001) 1947.

[11] J.Y. Li, X.L. Chen, H.li, M. He, Z.Y. Qiao, J. Cryst. Growth 233 (2001) 5.

[12] M.J. Zheng, L.D. Zhang, G.H. Li, W.Z. Shen, Chem. Phys.Lett. 263 (2002) 123.

[13] J.J. Wu, S. C. Liu, Adv.Mater. 14 (2002) 215.

[14] S. Baruah, J.Dutta, Sci. Technol. Adv. Mater. 10 (2009) 013001.

[15] P.Hari, M. Baumer, W.D Tennyson, L.A. Bumm, J. Non-Crystalline Solids 354 (2008) 2843

[16] B.OôRegen, M. Gratzel, Nature 353 (1993) 737

[17] E.M. Kaidadhev, M Lorenz, H. Wenckstern, H. Hochmuth, A. Rahm, H.C. Semmel-hack, K.H. Han, G. Benndorf, C.Bundesmann, H. Hochmuth, M. Grundmann, Appl. Phys. Lett. 82 (2003) 3901.